

Reference study to characterise plasma and magnetic properties of ultra-cool atmospheres

M. I. Rodríguez-Barrera^{1*}, Ch. Helling¹, C. R. Stark¹ and A. M. Rice^{1*†}

¹*SUPA, School of Physics & Astronomy, University of St. Andrews, St. Andrews KY16 9SS, UK*

12 February 2022

ABSTRACT

Radio and X-ray emission from brown dwarfs suggest that an ionised gas and a magnetic field with a sufficient flux density must be present. We perform a reference study for late M-dwarfs, brown dwarfs and giant gas planet to identify which ultra-cool objects are most susceptible to plasma and magnetic processes. Only thermal ionisation is considered. We utilise the DRIFT-PHOENIX model grid where the local atmospheric structure is determined by the global parameters T_{eff} , $\log(g)$ and $[M/H]$.

Our results show that it is not unreasonable to expect H_α or radio emission to origin from Brown Dwarf atmospheres as in particular the rarefied upper parts of the atmospheres can be magnetically coupled despite having low degrees of thermal gas ionisation. Such ultra-cool atmospheres could therefore drive auroral emission without the need for a companion’s wind or an outgassing moon. The minimum threshold for the magnetic flux density required for electrons and ions to be magnetised is well above typical values of the global magnetic field of a brown dwarf and a giant gas planet. Na^+ , K^+ and Ca^+ are the dominating electron donors in low-density atmospheres (low $\log(g)$, solar metallicity) independent of T_{eff} . Mg^+ and Fe^+ dominate the thermal ionisation in the inner parts of M-dwarf atmospheres. Molecules remain unimportant for thermal ionisation. Chemical processes (e.g. cloud formation) affecting the most abundant electron donors, Mg and Fe, will have a direct impact on the state of ionisation in ultra-cool atmospheres.

Key words: brown dwarfs, planets and satellites: atmospheres, stars: atmospheres, plasma, radio continuum: planetary systems, radio lines: planetary systems

1 INTRODUCTION

Ultra-cool objects like brown dwarfs and giant gas planets have masses below the hydrogen-burning limit of $\sim 0.08 M_\odot$ (e.g. Burrows et al. 2001). Brown dwarfs are born like stars by gravitational collapse, however, they have not sufficient mass to achieve the required core temperature to provide a steady rate of nuclear hydrogen fusion. As a consequence, gravitational collapse provides the only energy source for most of the brown dwarf’s lifetime. Cooling and contracting during their entire life, brown dwarfs cannot compensate the radiative losses by thermonuclear processes. Brown dwarfs evolve from a young objects with an effective temperature $T_{\text{eff}} \approx 3000$ K that is comparable to late M-dwarfs and surface gravities like giant gas planets to high-gravity objects of

$\log(g)=5.0$ with an effective temperature lower than $T_{\text{eff}} \approx 500$ K. Brown dwarfs are fully convective objects, and they can be fast rotators. Brown dwarfs and giant gas planets form clouds in their atmospheres which have strong feedback onto the atmospheric structure due to element depletion and due to a high opacity (Helling & Casewell 2014 and references there in). Observations by Biller et al. (2013), Buenzli et al. (2014) and Crossfield et al. (2014), for example, suggest that brown dwarf atmospheres show a patchy cloud coverage. Transit spectroscopy from extrasolar planets suggest that giant gas planets are covered in hazes and clouds too (Pont et al. 2008; Gibson et al. 2012; Sing et al. 2015). Model simulations suggest that cloud formation prevails for a large range of effective temperatures up to 2800 K, and for metallicities as low as $[M/H] = -5.0$ (Witte, Helling & Hauschildt 2009). A significant volume of these clouds is susceptible to local discharge events (Helling et al. 2013): large-scale discharges in the upper cloud regions and corona-like small-scale discharges in the inner, denser part of the cloud. These local discharge events may generate atmospheric electrical storms. At the same time, storms may ionise the local

* E-mail: mirb@st-andrews.ac.uk

† This file has been amended to highlight the proper use of $\LaTeX 2_\epsilon$ code with the class file. These changes are for illustrative purposes and do not reflect the original paper by M. I. Rodríguez-Barrera.

gas. Luque et al. (2014) modelled the ionosphere of Saturn and Jupiter finding that the atmospheric electrical storms may produce up to 10^3 cm^{-3} of free electrons below the ionosphere.

Radio and X-ray emission from ultra-cool dwarfs are now well established (e.g. 2MASSJ10475385+2124234 by Route & Wolszczan 2012; 2MASS J13153094-2649513AB by Burgasser et al. 2013). Berger (2002) observed twelve sources in radio, X-ray and H_α emission between the spectral types M8 and L3.5. Sorahana, Suzuki & Yamamura (2014) present mid-IR AKARI observations which suggest the presence of chromospheric activity in brown dwarfs. Schmidt et al. (2015) derive a rise in magnetic activity in form of H_α emission from SDSS spectra from 2% for early M-dwarfs (M0) to 88% for early L-dwarfs (L0). 39% of the L dwarfs in their sample observed multiple times are suggested to be variable. Such observations indicate that an appropriately ionised gas is present in the atmospheres of such cool objects that allows chromospheric heating. The prevailing question is how much of such a cool, cloud-forming atmosphere needs to be ionized that a chromosphere could form.

It is suggested that the magnetic field strength of brown dwarfs is as high as 10^3 G (e.g. Shulyak et al. 2011). Lynch, Mutel & Güdel (2015) suggest field strengths of $\sim 2.5 \dots 2.5 \text{ kG}$ for the surface field on TVLM 0513-46 and 2M 0746+20. A correlation between radio activity and rotation has not been settled for brown dwarfs given the wide parameter range occupied by these objects (McLean, Berger & Reiners 2012; Antonova et al. 2013). Williams et al. (2014) demonstrate that ultra-cool objects do not follow the classical Güdel-Benz relation where the X-ray and the radio luminosity from F – M stars correlate (Güdel & Benz 1993). This relation was shown to persist for solar flares and active rotating binaries (Benz & Güdel 1994). The deviation of ultra-cool stars from the Güdel-Benz relation beyond than approximately M5 may suggest a change in the dynamo mechanism that produces the magnetic field in such ultra-cool objects (Cook, Williams & Berger 2014). If the atmospheric gas can couple to the strong magnetic field in brown dwarfs, the kinetic energy carried by large-scale convective motions may be transported to the top of the atmosphere and released in form of flares, quiescent or quasi-quiescent emissions. The flares are a sudden release of magnetic energy from the deeper convective layers. The quiescent emission is a continuous emission but at lower energy levels than flares. The most likely mechanism to produce this emission is electron cyclotron maser emission from highly relativistic electrons or plasma emission alternatively, incoherent synchrotron or gyrosynchrotron emission from relativistic electrons (Hallinan et al. 2006). Flares and quiescent emission were reported for example by Burgasser & Putman (2005) for two late-type M-dwarfs, with a magnetic field strength of 1 kG. Tanaka, Suzuki & Inutsuka (2014) study the mass loss of hot Jupiters through MHD waves. They suggest the formation of a chromosphere by Alfvén wave heating. Tanaka, Suzuki & Inutsuka (2014), however, observe, that the gas does not need to be fully ionised, i.e. degree of ionisation $f_e < 1$, for the mechanism to work. Mohanty et al. (2002) analysed magnetic Reynolds number, $R_m \propto f_e$, for a set of model atmospheres to show why the chromospheric H_α activity should be low in rapid rotating brown dwarfs with $T_{\text{eff}} \geq 1500 \text{ K}$ and solar metallicity. The works by Schmidt

et al. (2015) and Sorahana, Suzuki & Yamamura (2014) suggest that L-dwarfs should have a chromosphere (but with a reduced filling factor) despite having low magnetic Reynolds numbers.

Our paper presents a theoretical framework using a set of fundamental parameters to analyse the ionisation and magnetic coupling state of objects with ultra-cool atmospheres. This paper focuses on late M-dwarfs, brown dwarfs and giant gas planets spanning $T_{\text{eff}} = 1000 \dots 3000 \text{ K}$. The approach is also applicable to, for example, protoplanetary disks. Only thermal ionisation is considered for this reference study against which the effect of additional processes (e.g. dust-dust collisions, cosmic ray ionisation, Alfvén ionisation, lighting, photoionisation) can be tested in future works. Our investigations utilise results from DRIFT-PHOENIX 1D model atmosphere simulations (Helling et al. 2008; Witte, Helling & Hauschildt 2009; Witte et al. 2011). This allows us to perform an extensive reference study across the late M-dwarf, brown dwarf and planetary regime on the basis of a consistently calculated model atmosphere grid for a large set of global parameters (T_{eff} , $\log(g)$, $[M/H]$). The aim of this study is to identify ultra-cool objects that are most susceptible to plasma processes by itself or that lead to instabilities that trigger the emergence of a strong plasma. This study does not include any multi-dimensional atmospheric flows and resulting multi-D radiative transfer effects.

Section 2 describes our approach and the use of the DRIFT-PHOENIX model atmosphere results. Sections 3 and 5 introduce our theoretical frame work in form of basic plasma and magnetic parameters, respectively. Our study shows that ultra-cool atmospheres are composed of an ionised and magnetised gas. The local degree of ionisation varies largely amongst the objects and throughout the atmospheres. While a late M-dwarf has a considerable degree of ionisation throughout the whole atmosphere, the degree of thermal ionisation for a L-dwarf is rather low but may well be enough to seed other ionisation processes like for example due to Alfvén ionisation (Stark et al. 2013). In Sec. 3.3.2 we demonstrate that electromagnetic interactions can dominate over electron-neutral interactions also in regions of a very low degree of ionisation. In Sec. 3.3.3 we investigate the relevant length scales effected by electrostatic interactions in the gas phase. Section 4 (with additional material in Appendix A) contains our assessment of the local equilibrium chemistry abundances with respect to electron donors species across the late M-dwarfs, brown dwarfs and giant planets regime.

In Sec. 5 we demonstrate that 30%-50% of the atmospheric volume can be magnetically coupled in L-dwarfs for a magnetic field strength of 10^3 G . The atmospheric volume with a degree of thermal ionisation above a plasma threshold value of $> 10^{-7}$ is, however, considerably lower. Our results show that it is not unreasonable to expect ultra-cool atmospheres to emit H_α or even in radio wavelength as in particular the rarefied upper parts of the atmospheres are affected by electromagnetic interactions over many pressure scale heights despite having low degrees of ionisation. Section 6 contains the discussion of our results in view of previous publications. Section 7 presents our conclusions.

Table 1. DRIFT-PHOENIX atmosphere structures used:**Group 1:** giant gas planets and young brown dwarfs.**Group 2:** dependence on $\log(g)$.**Group 3:** dependence on metallicity.

	T_{eff} [K]	$\log(g)$	[M/H]
Group 1	1000-3000	3.0	0.0
Group 2	1000 2000 2800	3.0, 4.0, 5.0	0.0
Group 3	1000 2000 2800	3.0	-0.6, -0.3, 0.0, +0.3

2 APPROACH

We aim to assemble a theoretical framework that allows us to assess the plasma and magnetic character in atmospheres of objects across the stellar-planetary boundary, namely for late M-dwarfs, brown dwarfs and planets. Our approach is not limited to these objects as the plasma parameters used are fundamental properties of a gas rather than of a particular object. We utilise the grid of DRIFT-PHOENIX model atmosphere structures in order to quantify the plasma and magnetic characteristics. DRIFT-PHOENIX is a combination of two complementary codes, DRIFT and PHOENIX (Helling et al. 2008; Witte, Helling & Hauschildt 2009; Witte et al. 2011). The DRIFT code (Woitke & Helling 2004; Helling et al. 2008) solves a system of equations that describes the stationary dust formation process of mineral clouds (seed formation, growth, evaporation, sedimentation, element depletion) and interaction between the dust grains and gas (Woitke & Helling 2003, 2004; Helling & Woitke 2006; Helling, Woitke & Thi 2008). PHOENIX is a hydrostatic radiative transfer model atmosphere code (Hauschildt & Baron 1999) that determines the resultant thermodynamic structure of the atmosphere (local gas temperature T_{gas} [K], local gas pressure p_{gas} [bar] and local electronic pressure p_e [bar]) from fundamental stellar parameters (effective temperature T_{eff} [K], surface gravity $\log(g)$ [cm s^{-2}] and metallicity [M/H]). When combined with DRIFT it provides a self-consistent atmospheric model that takes into account cloud formation and its impact on the thermodynamic structure and the resulting spectral energy distribution.

The DRIFT-PHOENIX atmosphere simulations model the kinetic formation of mixed mineral cloud particle made of $\text{TiO}_2[\text{s}]$, $\text{Al}_2\text{O}_3[\text{s}]$, $\text{Fe}[\text{s}]$, $\text{SiO}_2[\text{s}]$, $\text{MgO}[\text{s}]$, $\text{MgSiO}_3[\text{s}]$, $\text{Mg}_2\text{SiO}_4[\text{s}]$ which effects 6 elements (O, Mg, Si, Fe, Al, Ti). Mg, Si, and Fe are the most abundant elements after O and C in a gas with solar element abundances.

Using DRIFT-PHOENIX atmospheric models with a range of effective temperatures ($T_{\text{eff}} = 1000 \text{ K} - 3000 \text{ K}$), surface gravity ($\log(g) = 3.0, 4.0, 5.0$) and metallicity ([M/H] = -0.6, -0.3, 0.0 +0.3), we evaluate the degree of thermal gas ionisation, the plasma parameter (Sec. 3) and magnetic parameters (Sec. 5). Applying a separate chemical equilibrium code, we evaluate the gas-phase composition of various atmosphere models to assess if the dominating electron donating species changes or remains the same (Sec. 4.1).

We apply a chemical equilibrium routine to calculate

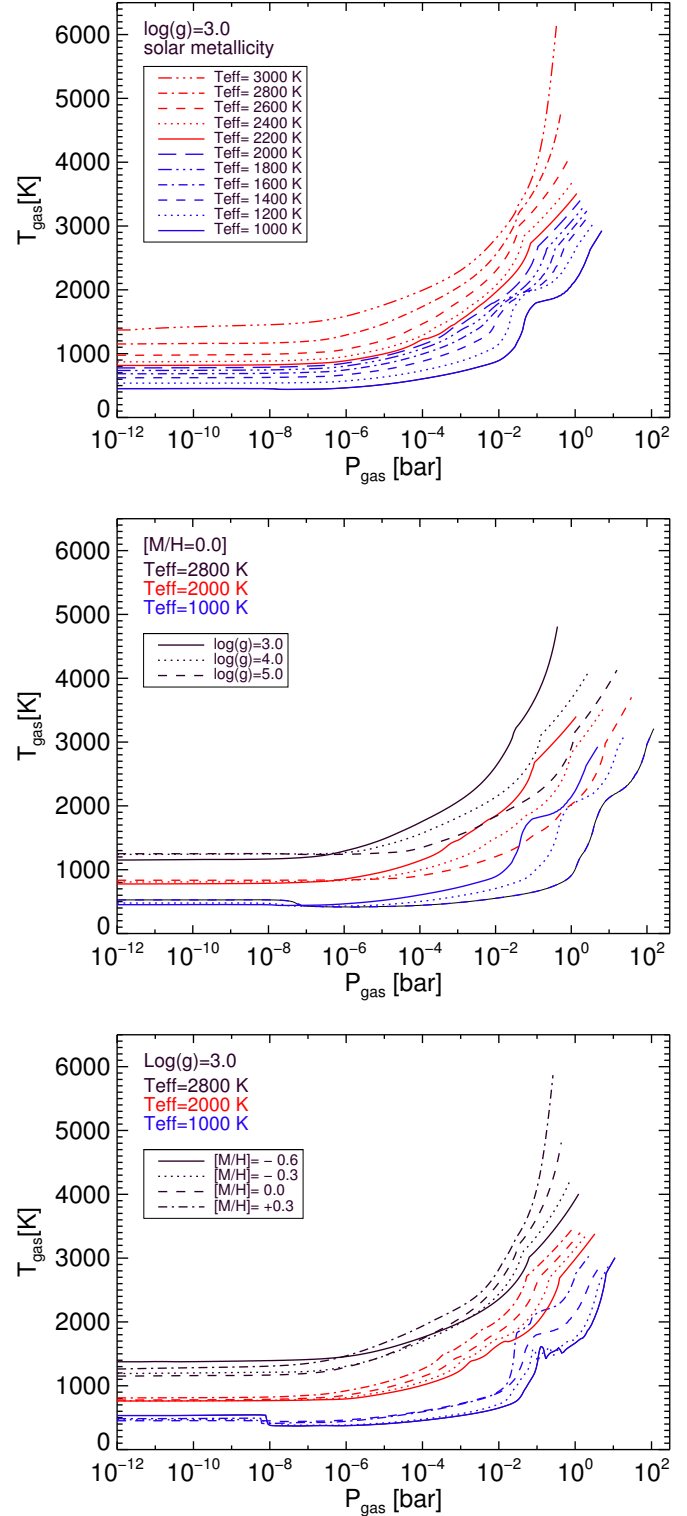


Figure 1. ($T_{\text{gas}}-P_{\text{gas}}$) input structure from the DRIFT-PHOENIX model atmosphere grid. The hottest models represent late M-dwarf atmospheres or atmospheres of young brown dwarfs. The coolest models represent atmospheres in the planetary regime. **Top:** Group 1. **Middle:** Group 2. **Bottom:** Group 3.

the chemical composition in more detailed than available from the standard DRIFT-PHOENIX output. Our main interest is to evaluate the results regarding the ions in the gas phase. A combination of 155 gas-phase molecules (including 33 complex hydrocarbon molecules), 16 atoms, and various ionic species were used under the assumption of local thermodynamic equilibrium (LTE). The Grevesse, Asplund & Sauval (2007) solar composition is used for calculating the gas-phase chemistry outside the metal depleted cloud layers. No solid particles were included in the chemical equilibrium calculations but their presence influences the gas phase by the reduced element abundances due to cloud formation and the cloud opacity impact on the radiation field, both accounted for in the DRIFT-PHOENIX model simulations.

We utilize DRIFT-PHOENIX model atmosphere (T_{gas} , p_{gas} , p_e) structures and the dust element depleted abundances as input for our calculations. We group the DRIFT-PHOENIX atmosphere structures into three groups for an easier presentation of our results (Table 1). These groups, defined by a range of global parameters, cover young and old giant gas planets, young and old brown dwarfs and late M-dwarfs. Figure 1 shows the thermodynamic profiles (T_{gas} , p_{gas}) for each of these groups. As the effective temperature increases, the thermodynamic gas temperature of the atmosphere increases as well for a given $\log(g)$ and $[M/H]$. The effect of dust on the local gas temperature in the atmosphere appears as a step-like temperature change (backwarming) in the atmosphere models.

3 BASIC PLASMA PARAMETERS

In the following section, we lay out the theoretical framework that we use to characterise the plasma of an atmospheric environment with respect to its electrostatic and magnetostatic behaviour. This is inspired by the wealth of radio observations of substellar objects (Berger 2002; Berger et al. 2010; Route & Wolszczan 2012; Burgasser et al. 2013; Williams et al. 2014). To understand these observations, radio wavelength (quiescent emission) and X-ray emission (flares), the atmospheric gas must couple with the background magnetic field. As a consequence, free charged particles produced in the atmosphere would be accelerated along magnetic field lines and released into the upper parts of the atmosphere. A magnetic coupling of the local gas would also be required for Alfvén waves to develop and potentially contributing to an acoustic heating of a chromosphere also on such ultra-cool objects (e.g. Testa, Saar & Drake 2015). We note that ideal and non-ideal MHD simulations require a certain degree of ionisation to allow Alfvén wave heating to develop as possible mechanisms for chromospheric heating.

For a plasma to exist, the gas needs to be ionised. The degree of ionisation, f_e measures the extent to which a gas is ionised, and it is defined as

$$f_e = \frac{p_e}{p_e + p_{\text{gas}}}, \quad (1)$$

where p_{gas} and p_e are the gas and electron pressure respectively, both in [bar]. Once we have determined the degree of ionisation of the atmospheric gas depending on the global parameters (T_{eff} , $\log(g)$, $[M/H]$) we evaluate the plasma frequency to investigate where in the atmosphere electromagnetic interactions dominate over kinetic collisions between

electrons and neutrals,

$$\omega_{\text{pe}} \gg \nu_{\text{ne}}. \quad (2)$$

ω_{pe} [rad s⁻¹] is the plasma frequency (i.e. the frequency at which the plasma reacts to an imposed or perturbed electric fields), ν_{ne} [s⁻¹] is the electron-neutral collision frequency. Only if Eq. 2 is fulfilled, we can expect the ionised gas to undergo electromagnetic interactions that could lead, for example, to discharge processes. A more refined insight about electrostatic interactions influencing the atmospheric gas can be gained by determining the length scales beyond which the Coulomb force of a charge does not any more effects its surrounding. On length-scale larger than the Debye length, a gas will be quasi-neutral and no electrostatic forces will effect the gas behaviour. Hence,

$$\lambda_D \ll L \quad (3)$$

with λ_D the Debye length and L the typical length scale of the considered plasma, both in [m]. Ideally, this would be associated with the atmospheric volume where the ionised gas can couple to an external magnetic field.

In the following subsections we define each of the plasma criteria and evaluate them for our model atmosphere grid. All equations and natural constants are given in SI units. All results, however, have been converted into cgs unit for an easier representation in the astrophysical context.

3.1 Plasma Frequency: $\omega_{\text{pe}} \gg \nu_{\text{ne}}$

In a plasma, if electrons are displaced from their equilibrium position (assuming a uniform, stationary ionic background), a charge imbalance is imposed on the plasma, creating a local, restoring electric field. Consequently, the electrons try to re-establish charge neutrality resulting in them oscillating around their equilibrium position with a particular frequency called plasma frequency. The plasma frequency is defined as,

$$\omega_{\text{pe}} = \left(\frac{n_e e^2}{\epsilon_0 m_e} \right)^{1/2}, \quad (4)$$

with n_e the electron number density [m⁻³], e the electron charge [C], m_e the electron mass [kg]. If the plasma frequency, ω_{pe} , is greater than the frequency of collisions between the electrons and neutral particles, ν_{ne} [s⁻¹] then, long-range electromagnetic collective effects dominant over short-range binary interactions (see Fig. 3). The collision frequency for neutral particles with electrons is given by $\nu_{\text{ne}} = \sigma_{\text{gas}} n_{\text{gas}} v_{\text{th,e}}$, where $v_{\text{th,e}}$ is the thermal velocity of electrons given by $v_{\text{th,e}} = (k_B T_s / m_s)^{1/2}$ [m s⁻¹], n_{gas} the ambient gas density and σ_{gas} the collision, or scattering, cross section of particles. The latter is assumed to be $\sigma_{\text{gas}} = \pi \cdot r_{\text{gas}}^2$ with $r_{\text{gas}} = r_{\text{H}_2}$ as the atmospheric gas in late M-dwarfs, brown dwarfs and most likely in giant gas planets is composed mostly of molecular hydrogen, H₂. Therefore, the collision cross section is approximated by $\sigma_{\text{gas}} \approx \sigma_{\text{H}_2} \approx \pi \cdot r_{\text{H}_2}^2 = 5.81 \cdot 10^{-20}$ m² ($r_{\text{H}_2} = 1.36 \cdot 10^{-10}$ m). If the charged particles collide frequently with the ambient neutral gas ($\omega_{\text{pe}} / \nu_{\text{ne}} < 1$), their motion will be determined by nearest neighbour interactions and not by collective, long-range electromagnetic interactions.

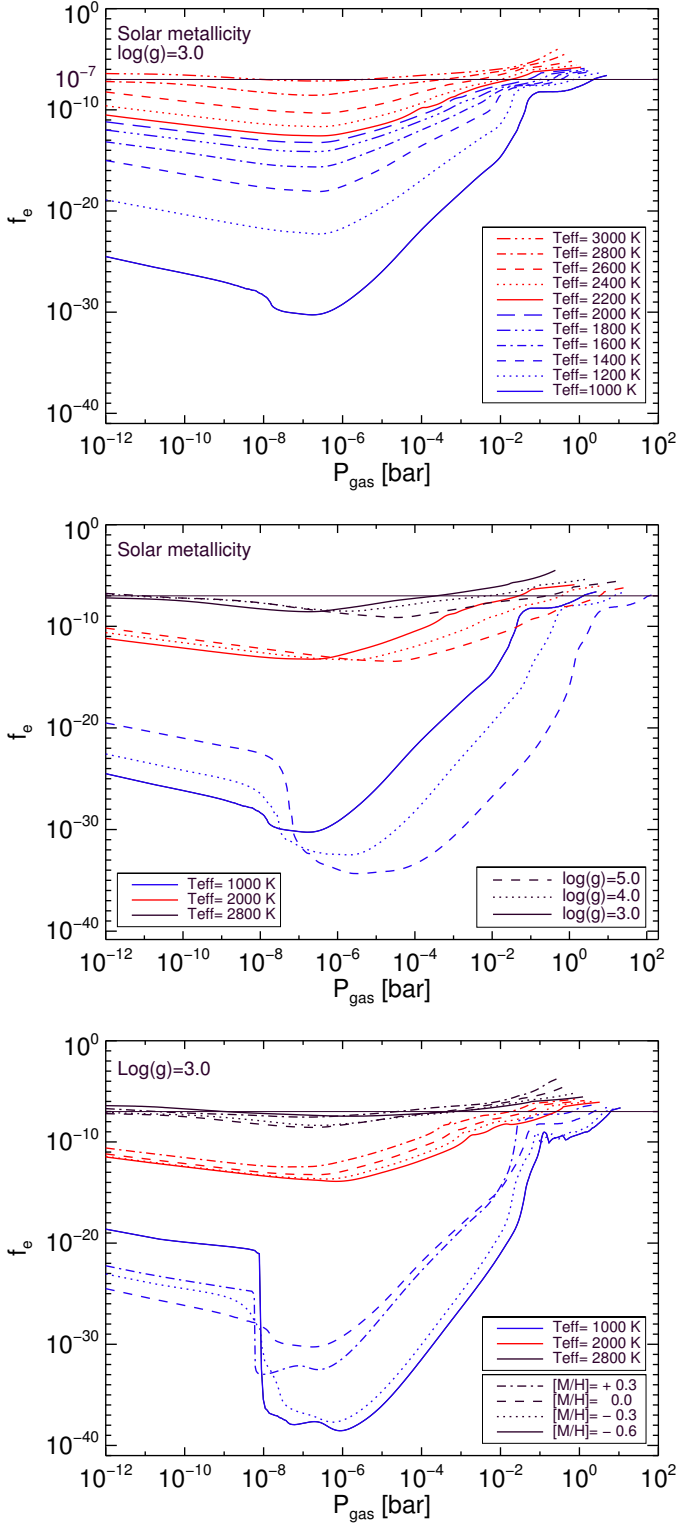


Figure 2. The degree of thermal ionisation, $f_e = p_e / (p_e + p_{\text{gas}})$ as a measure of free charged particles for M-dwarf, brown dwarf and giant gas planet atmospheres. The M-dwarf atmosphere is easily ionised by thermal processes. Atmosphere of brown dwarfs can only be thermally ionised in deeper layers. **Top:** Group 1. **Middle:** Group 2. **Bottom:** Group 3.

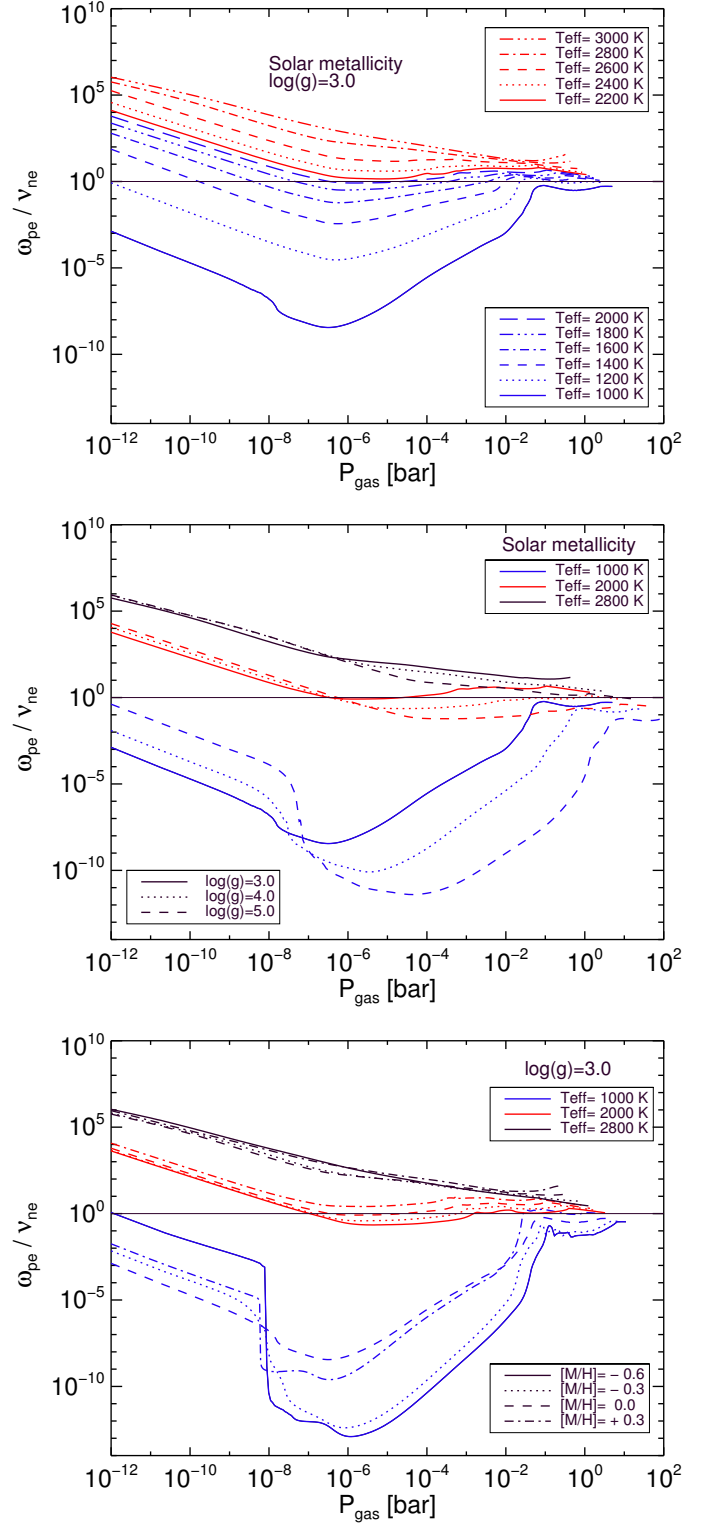


Figure 3. Ratio of plasma frequency of the electrons and the frequency of collisions between neutral particles and electrons. Electromagnetic interactions dominate over electron-neutral interactions if $\omega_{pe} / \nu_{ne} \gg 1$. **Top:** Group 1. **Middle:** Group 2. **Bottom:** Group 3.

3.2 Debye length: $\lambda_D \ll L$

The Debye length, λ_D , is the spatial length scale beyond which a plasma can be considered quasi-neutral ($n_e \approx n_i \approx n_{\text{gas}}$). For length scales less than the Debye length, a test charge will experience the influence of the charge imbalance inside the Debye sphere. The Debye length, λ_D [m], resulting from the solution of the Poisson equation for a non-zero charge density near test charge, is defined as

$$\lambda_D = \left(\frac{\epsilon_0 k_B T_e}{n_e e^2} \right)^{1/2}. \quad (5)$$

with $k_B = 1.38 \times 10^{-23}$ [J K⁻¹] and $\epsilon_0 = 8.85 \times 10^{-12}$ [F m⁻¹]. A plasma is quasi-neutral if

$$\lambda_D \ll L. \quad (6)$$

For an ionised gas region to exhibit plasma behaviour, it is required that over the length scale of the region, the electron number density is high enough that L is greater than the Debye length. The typical length scale of the plasma, L [m], considered in the literature (e.g. Mohanty et al. 2002; Tanaka, Suzuki & Inutsuka 2014) is the pressure scale height which depends on the local gas properties and varies with $1/g$. Typical values for the pressure scale height are $10^5 \dots 10^6$ cm for a brown dwarf with $\log(g) = 5$. Tanaka, Suzuki & Inutsuka (2014) base their length scale on the definition of the Alfvén speed that is of the order of the velocity of sound (their Eq.12). Also their approach results in a typical length scale of the order of the pressure scale height. Associate with the Debye length is the number of charges inside a Debye sphere, N_D (*plasma parameter*, App. B). If $N_D \gg 1$, the ionised gas exhibits plasma behaviour.

3.3 Plasma parameters across the star-planet regime

In the following, we evaluate the plasma criteria for late M-dwarfs, brown dwarfs and giant gas planet atmospheres. All results have been calculated considering thermal ionisation only and compose our reference study against which the need for additional ionisation processes can be derived. First we examine for which global parameters and p_{gas} values, the gas is ionised above the threshold value of $f_e > 10^{-7}$ (Sec. 3.3.1). In Sec. 3.3.2 we demonstrate that long-range electromagnetic collective interactions of many charged particles can dominate over short-range binary interactions also in regions of a very low degree of ionisation. Recent brown dwarf atmospheric investigations have focused on the degree of ionization to characterize plasma behaviour, in this paper we consider multiple parameters to gain a more detailed characterization. (e.g. Osten et al. 2015). In Sec. 3.3.3 we demonstrate for which length scale ultra-cool atmospheres will be effected by electrostatic processes and that it is not unreasonable to expect ultra-cool atmospheres to emit H α or even in radio wavelength as in particular the rarefied upper parts of the atmospheres fulfill plasma criteria easily despite having low degrees of ionisation.

3.3.1 Degree of ionisation by thermal processes, f_e

Figure 2 shows the degree of thermal ionisation evaluated for the same models represented in Fig. 1 (Table 1). Guided

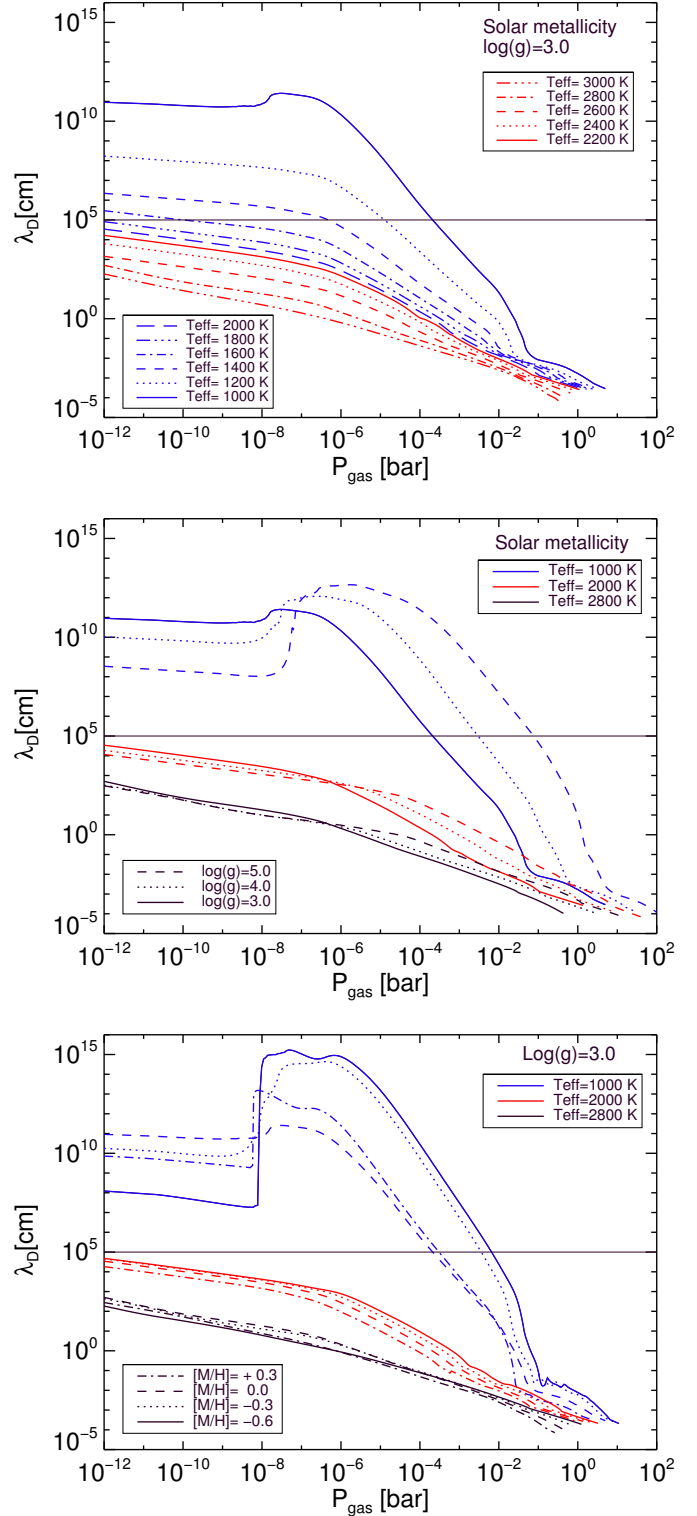


Figure 4. Debye length versus the local gas pressure assuming $T_e = T_{\text{gas}}$. For length scales less than the Debye length, a test charge will experience the influence of the charge imbalance inside the Debye sphere. The horizontal line indicates the typical length scale of the plasma $L=10^3$ m consider in this study (Helling et al. 2011). **Top:** Group 1. **Middle:** Group 2. **Bottom:** Group 3.

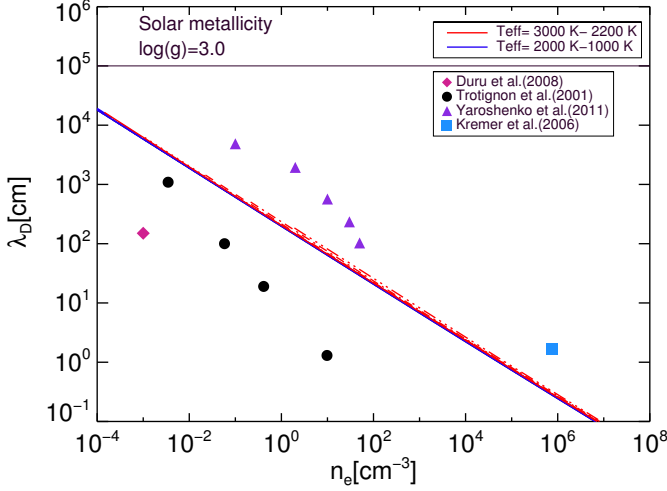


Figure 5. Comparison Debye length of different astrophysical environments Group1 (Table 1) is plotted here. The red lines represent $T_{\text{eff}} = 3000 \text{ K} - 2200 \text{ K}$ covering M-dwarfs and young L-dwarfs. Blue lines represent $T_{\text{eff}} = 2000 \text{ K} - 1000 \text{ K}$ covering late L-dwarfs and giant gas planets regime. The Debye lengths for Martian's atmosphere are plotted as red diamond (Duru et al. 2008) and black circle (Trotignon et al. 2001), for plasma composed of electrons, water group ions and protons as violet triangle (Yaroshenko et al. 2011) and a pure electron plasma as light blue square symbols (Kremer et al. 2006). The black line represents the typical atmospheric length scale, $L = 10^3 \text{ m}$ (Helling et al. 2011)

by these results we consider $f_e > 10^{-7}$ to be a threshold above which the gas is partially ionised and it may exhibit plasma behaviour. The above choice of a threshold value is supported by results from laboratory experiments and laboratory plasma devices (e.g. Tokamak; Diver 2001; Fridman 2008). For a fluorescent tube, the degree of ionisation is $f_e \approx 10^{-5}$ according to Inan & Golkowski (2010). Christophorou & Olthoff (2004) showed that at low temperature ($T_{\text{gas}} \approx 300 - 600 \text{ K}$) and low density ($10^{13} - 10^{16} \text{ cm}^{-3}$) the gas is weakly ionised with $f_e \approx 10^{-6} - 10^{-1}$. If the density of the charged particles increases towards $f_e \rightarrow 1$ the gas will be fully ionised. For example, a fully ionised gas is assumed in ideal MHD calculations. This threshold, $f_e > 10^{-7}$, allows us to derive the atmospheric volume that can be considered as an ionised gas (Sect. 3.4, Fig. 9). Deriving such atmospheric volume fractions will enable us to compare the results from different plasma criteria (Eqs. 2, 3) and to demonstrate that a gas does not need to be fully ionised in order to exhibit collective plasma effects.

• **Group 1: changing T_{eff} (Fig. 2, top)**
($\log(g)=3.0$, $[M/H]=0.0$)

A solar-metallicity M-dwarf with $T_{\text{eff}} = 3000 \text{ K}$ achieves $f_e > 10^{-7}$ in almost the entire atmosphere. For cooler atmospheres with $T_{\text{eff}} \leq 2800 \text{ K}$, $f_e > 10^{-7}$ is only reached for $p_{\text{gas}} > 10^{-4} \text{ bar}$. The atmospheric fraction that reached $f_e > 10^{-7}$ increases with increasing T_{eff} .

• **Group 2: changing $\log(g)$ (Fig. 2, middle)**
($T_{\text{eff}} = 1000 \text{ K}, 2000 \text{ K}, 2800 \text{ K}$, $[M/H]=0.0$)

Values of varying surface gravity $\log(g) = 3.0, 4.0, 5.0$ are studied here. Models with $T_{\text{eff}} = 2800 \text{ K}$ reach $f_e > 10^{-7}$

for $p_{\text{gas}} > 10^{-4} \text{ bar}$; models with $T_{\text{eff}} = 2000 \text{ K}$ for $p_{\text{gas}} > 10^{-2} \text{ bar}$. A small part of the upper atmospheric reaches $f_e > 10^{-7}$ for $T_{\text{eff}} = 2800 \text{ K}$ and $\log(g) = 4.0, 5.0$ due to the increasing contribution of Ca^+ with outwards decreasing p_{gas} (compare Fig. 6). Models with $T_{\text{eff}} = 1000 \text{ K}$ have only a small fraction of the atmospheric gas that reaches the $f_e > 10^{-7}$ threshold. This occurs in the deepest layers of the atmosphere $1 < p_{\text{gas}} < 10^2 \text{ bar}$. The atmospheric fraction that reached $f_e > 10^{-7}$ increases with decreasing $\log(g)$ at high p_{gas} and with increasing $\log(g)$ at low p_{gas} .

• **Group 3: changing $[M/H] = 0.0$ (Fig. 2, bottom)**
($T_{\text{eff}} = 1000 \text{ K}, 2000 \text{ K}, 2800 \text{ K}$, $\log(g)$)

Values of varying metallicity $[M/H] = -0.6, -0.3, 0.0, +0.3$ are analysed. Models with $T_{\text{eff}} = 2800 \text{ K}$ and $T_{\text{eff}} = 2000 \text{ K}$ satisfy $f_e > 10^{-7}$ for all values of metallicity for $p_{\text{gas}} > 10^{-5} \text{ bar}$. A small part of the upper atmosphere reaches $f_e > 10^{-7}$ for $T_{\text{eff}} = 2800 \text{ K}$ due to an increasing electron donation from Ca^+ . Models with $T_{\text{eff}} = 1000 \text{ K}$ have only a small fraction of the atmospheric gas that can be ionised for $p_{\text{gas}} > 10^{-1} \text{ bar}$.

All models of non-irradiated atmospheres show a degree of ionisation which increases from a minimum ($p_{\text{gas}} \sim 10^{-8} - 10^{-6} \text{ bar}$) with increasing local gas pressure values towards the deeper layers of the atmosphere. Atmosphere models with $T_{\text{eff}} \leq 2800 \text{ K}$, $\log(g) = 3.0$, $[M/H] = 0.0$ can reach $f_e > 10^{-7}$ only for high p_{gas} (inner parts of the atmosphere). Only one model atmosphere achieves $f_e > 10^{-7}$ throughout nearly the entire atmosphere ($T_{\text{eff}} = 3000 \text{ K}$, $\log(g) = 3.0$, $[M/H] = 0.0$). For atmospheres of late M-dwarfs, brown dwarfs and giant gas planets for $T_{\text{eff}} = 1000 \dots 3000 \text{ K}$ for varying $\log(g)$ and metallicity, we observe that:

- The hottest model has the highest thermal degree of ionisation, f_e .
- The lowest value of surface gravity causes an increase of f_e at high p_{gas} , however, the highest value of surface gravity causes an increase of f_e at low p_{gas} . Both trends are for a given T_{eff} and $[M/H]$.
- The highest metallicity values cause an increase of f_e at high p_{gas} compared to the lowest metallicity models. For $T_{\text{eff}} = 2800 \text{ K}$ and $T_{\text{eff}} = 1000 \text{ K}$ the lowest value of the metallicity causes an increase of f_e at low p_{gas} . Both trends are for a given T_{eff} and $\log(g)$.

Section 4 investigates which atoms or molecules are the most important electron donors in these cold atmospheres, and hence, responsible for the values of the degree of thermal ionisation, f_e . We note that the degree of thermal ionisation will be influenced by the formation of clouds if the dominating electron donors are amongst the most abundant condensing species. Ca does not fall into this category.

3.3.2 Dominating electromagnetic interaction

The criterion $\omega_{\text{pe}} \gg \nu_{\text{ne}}$ is used to derive where in an ultra-cool atmosphere the long-range, electromagnetic, collective interactions of many charged particles dominates over short-range binary interactions in a ionised gas of a certain degree of ionisation. Figure 3 shows the results of this criterion for the three groups of model atmosphere structures (Fig. 1).

- **Group 1: changing T_{eff} (Fig. 3, top)**

($\log(g)=3.0$, $[M/H]=0.0$)

As T_{eff} increases, the range of the p_{gas} where $\omega_{\text{pe}} \gg \nu_{\text{ne}}$ increase too. For models with $T_{\text{eff}} \geq 2200$ K the entire atmosphere satisfies this criterion; for $T_{\text{eff}} = 2000$ K almost the entire atmosphere; for models with $T_{\text{eff}} = 1800 - 1400$ K in the uppermost and for the innermost parts of the atmosphere and for $T_{\text{eff}} = 1200$ K only for $10^{-2} < p_{\text{gas}} < 10^{-1}$ bar. The model with $T_{\text{eff}} = 1000$ K is too cool to fulfill this criterion.

- **Group 2: changing $\log(g)$ (Fig. 3, middle)**

($T_{\text{eff}} = 1000$ K, 2000 K, 2800 K, $[M/H]=0.0$)

Models with $T_{\text{eff}} = 2800$ K satisfy this criterion throughout the whole atmosphere except for $\log=5.0$ at the highest pressures. For $T_{\text{eff}} = 2000$ K and $\log(g)=3.0$ almost the entire atmosphere fulfills this criterion; $T_{\text{eff}} = 2000$ K and $\log(g)=4.0$ only in the uppermost and for the innermost parts of the atmosphere; for $T_{\text{eff}} = 2000$ K and $\log(g)=5.0$ only for $p_{\text{gas}} < 10^{-6}$ bar. Models with $T_{\text{eff}} = 1000$ K do not satisfy the criterion.

- **Group 3: changing $[M/H]=0.0$ (Fig. 3, bottom)**

($T_{\text{eff}} = 1000$ K, 2000 K, 2800 K, $\log(g)$)

Models with $T_{\text{eff}} = 2800$ K and all value of metallicity and $T_{\text{eff}} = 2000$ K with $[M/H] = +0.3$ satisfy this criterion in the whole atmosphere. For $T_{\text{eff}} = 2000$ K and $[M/H] = 0.0$ almost the entire atmosphere fulfills this criterion. For $T_{\text{eff}} = 2000$ K and $[M/H] = -0.3, -0.6$ only in the uppermost and for the innermost parts of the atmosphere, $10^{-7} > p_{\text{gas}} > 10^{-3}$; models with $T_{\text{eff}} = 1000$ K and $[M/H] = +0.3$ only for $10^{-2} < p_{\text{gas}} < 10^0$. Models with $T_{\text{eff}} = 1000$ K and $[M/H] = 0.0, -0.3, -0.6$ and do not fulfill this criterion for any atmospheric gas pressure.

Figure 3 demonstrates that the collective, long-range electromagnetic interactions dominate over short-range binary interactions in atmospheres of low degrees of ionisations, i.e. for $2800 \geq T_{\text{eff}} \geq 2000$ K. As T_{eff} and the metallicity increase, $\omega_{\text{pe}} \gg \nu_{\text{ne}}$ is easier fulfilled at high p_{gas} , however, as T_{eff} increases and the metallicity decreases, $\omega_{\text{pe}} \gg \nu_{\text{ne}}$ is easier fulfilled at low p_{gas} for $T_{\text{eff}} = 2800$ K, 1000 K. This effect is counteracted by an increase in $\log(g)$. The lowest value of $\log(g)$ causes a decrease of $\omega_{\text{pe}}/\nu_{\text{ne}}$ in the uppermost parts of the atmosphere and an increase in the innermost parts. Consequently, long-range, electromagnetic, collective interactions of many charged particles do not require a complete ionisation of the atmospheric gas, and a moderate gas ionisation is sufficient.

3.3.3 Electrostatically effected atmospheric length scales

The Debye length, λ_D , is compared to a typical atmospheric length scale of the order of the pressure scale height, $L=10^3$ m (Helling et al. 2011). Figure 4 shows how the Debye length changes depending on the local atmospheric gas pressure, and where $\lambda_D \ll L$ is fulfilled.

- **Group 1: changing T_{eff} (Fig. 3, top)**

($\log(g)=3.0$, $[M/H]=0.0$)

The criterion $\lambda_D \ll L$ is fulfilled throughout the whole atmosphere for $T_{\text{eff}} \geq 1800$ K; only for $T_{\text{eff}} = 1600$ K a small atmospheric gas volume for $p_{\text{gas}} < 10^{-10}$ bar cannot reach

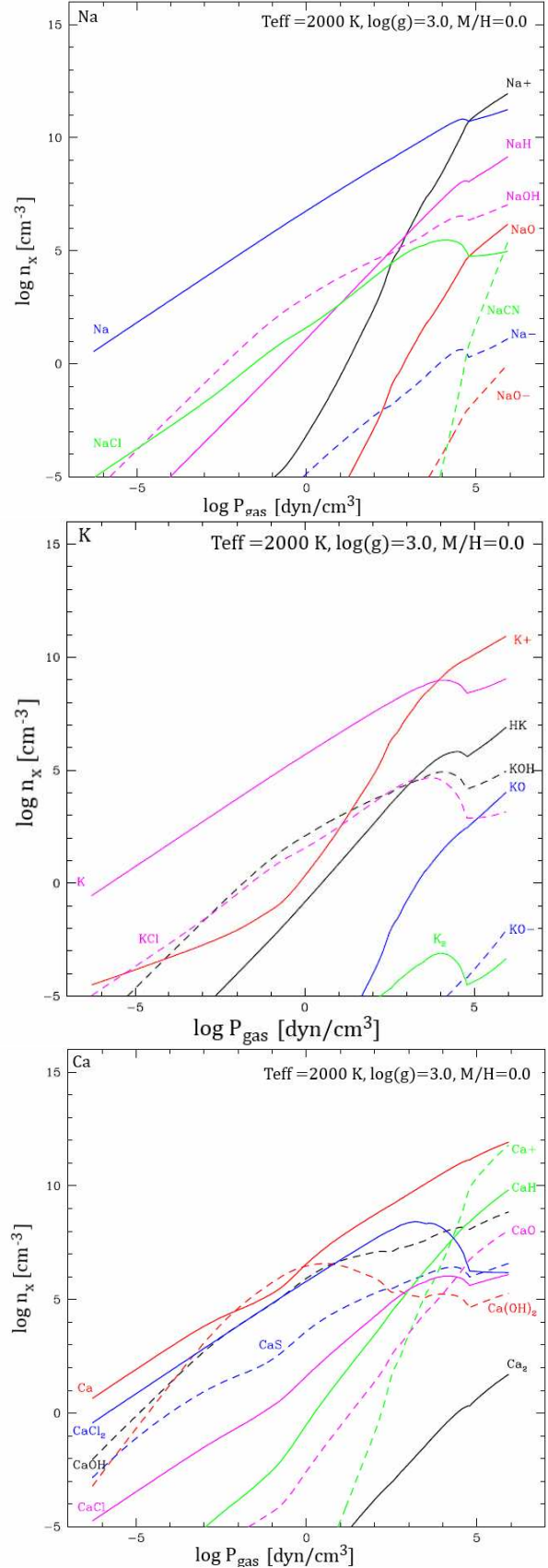


Figure 7. Distribution of electron donor's abundance over atoms, molecules and ions for a warm model of $T_{\text{eff}} = 2000$ K, $\log(g)=3.0$ and solar element composition. The upper left corner contains the element considered.

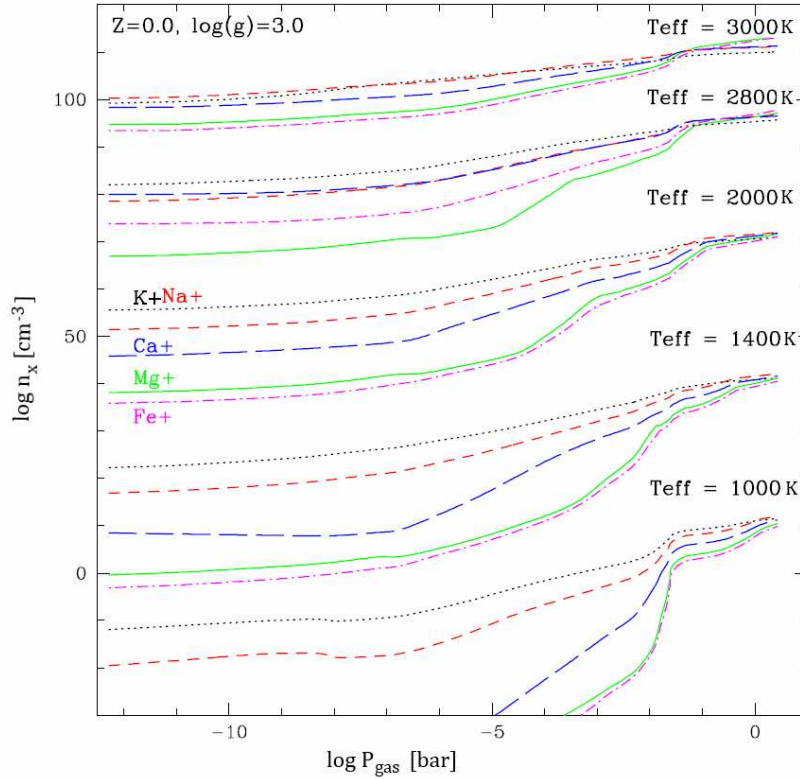


Figure 6. The dominating thermal electron donors for a subset of effective temperatures for $\log(g)=3.0$ and solar element abundances; Na^+ , K^+ and Ca^+ in the low-density atmosphere for all T_{eff} ; Mg^+ and Fe^+ in the inner parts for $T_{\text{eff}} \geq 2800$ K. An off-set of 3 orders of magnitudes is applied between the models for all $T_{\text{eff}} > 1000$ K to allow a better comparison.

this criterion. For models with $T_{\text{eff}} \leq 1400$ K this criterion is fulfilled for $p_{\text{gas}} > 10^{-6}$ bar. As T_{eff} increases, the range of p_{gas} where $\lambda_D \ll L$ increases.

- **Group 2: changing $\log(g)$ (Fig. 3, middle)**

($T_{\text{eff}} = 1000$ K, 2000 K, 2800 K, $[\text{M}/\text{H}] = 0.0$)

Models with $T_{\text{eff}} = 2800$ K and 2000 K satisfy this criterion for all surface gravity values and throughout the whole atmosphere. For $T_{\text{eff}} = 1000$ K and all surface gravity values then $\lambda_D \ll L$ is fulfilled only for $p_{\text{gas}} > 10^{-4}$ bar.

- **Group 3: changing $[\text{M}/\text{H}] = 0.0$ (Fig. 3, bottom)**

($T_{\text{eff}} = 1000$ K, 2000 K, 2800 K, $\log(g)$)

Models with $T_{\text{eff}} = 2800$ K and 2000 K satisfy this criterion for all metallicities and p_{gas} . Models with $T_{\text{eff}} = 1000$ K satisfy this criterion in the inner atmospheric regions only where $p_{\text{gas}} > 10^{-4}$ bar.

Figure 4 demonstrates that the Debye length is generally very large in the upper atmospheric regions throughout the whole regime of ultra-cool objects, i.e. late M-dwarfs, brown dwarfs and giant gas planets. In the upper atmosphere the electron density is low causing an increasing Debye length; whereas deeper in the atmosphere the electron number density is high and so the Debye length is relatively lower. According to Cravens (1997), at the top of the Earth's ionosphere $\lambda_D \approx 1$ cm for $T_e \approx 1000$ K and $n_e \approx 10^{11} \text{ cm}^{-3}$, compared to a vertical extent of ≈ 300 km of the ionosphere. For the solar wind at ≈ 1 AU, $\lambda_D \approx 700$ cm ($T_e \approx 10^5$ K,

$n_e \approx 10^7 \text{ cm}^{-3}$). A comparison of different values of the Debye sphere for different astrophysical environments is presented in Table 2 and in Fig. 5. Duru et al. (2008) investigate the electron density in the upper ionosphere of Mars, Trotignon et al. (2001) the interaction of the Martian's atmosphere with the solar wind. Both consider the presence of the dust in the plasma environment. Yaroshenko et al. (2011) model a plasma composed of electrons, water group ions and protons with the presence of photoemission due to the UV radiation. Kremer et al. (2006) work with a pure electron plasma.

Section B provides supplementary material about N_D , the average number of charges in the Debye sphere. The values for N_D are $\gg 10^5$ in the rarefied upper part of the atmospheres ($p_{\text{gas}} < 10^{-4}$ bar) for all M-dwarf, brown dwarf and giant gas planet model atmospheres investigated here. Values for the above quoted Debye length for the Earth ionosphere and solar wind are $N_D^{\text{ionosphere}} = 10^5$ and $N_D^{\text{solarwind}} = 10^{10}$. The parameter N_D indicates that the gas is dominated by many long-range interactions of charged particles, rather than the short-range binary interactions. If any charged particle is close enough to others then, it interacts in a collective behaviour, not only with the closest one. This collective behaviour distinguishes a plasma from a kinetic gas. Collective behaviour occurs if $N_D \gg 1$. Figure B1 shows that $N_D \gg 1$ is satisfied throughout the whole atmosphere for model atmosphere structures presented in Table 1. A substantially higher N_D is required for cooler at-

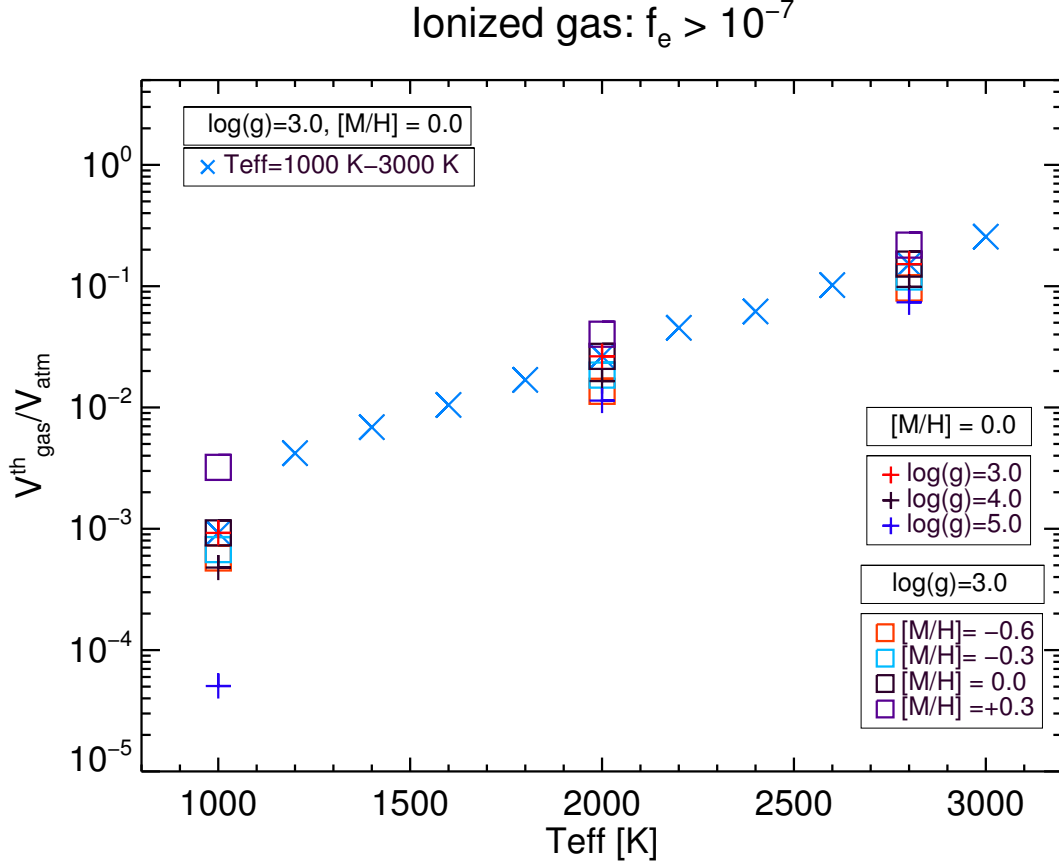


Figure 9. The fraction of the thermally ionized atmospheres volume, $V_{\text{gas}}^{\text{th}}/V_{\text{atm}}$, for $f_e > 10^{-7}$ and for M-dwarf, brown dwarf and giant planet atmospheres.

Table 2. Debye lengths for different astrophysical environments. Figure 5 provides a comparison to results of these papers.

Object	T_e [K]	n_e [cm^{-3}]	λ_D [cm]	References
Martian's Ionosphere	5000	10^{-3}	1.5×10^2	Duru et al. (2008) (Mar's atmosphere)
Martian's Ionosphere	347 3131 12222 86665	9.78 4.12×10^{-1} 5.82×10^{-2} 3.47×10^{-3}	1.3 19 10^2 1.1×10^3	Trotignon et al. (2001) (Mar's atmosphere)
Saturn Orbit Insertion	1.16×10^4 3×10^4 7×10^4 1.7×10^5 4×10^5	50 30 10 2 0.1	10^2 2×10^2 5.6×10^2 1.9×10^3 5×10^3	Yaroshenko et al. (2011) (electron, water group ions and protons plasma)
Laboratory Experiments	46418	7.5×10^6	1.7	Kremer et al. (2006) (pure electrons plasma)

mospheres than in atmospheres for higher T_{eff} if thermal ionisation is considered only (i.e. $T_e = T_{\text{gas,LTE}}$).

3.4 Comparing different plasma criteria

Radio and X-ray observations from low-mass objects suggest that their atmospheres contain enough free charges to constitute a magnetized plasma (Hallinan et al. 2008). From our evaluation of the thermal degree of ionisation (Sect. 3.3.1), we chose a threshold for the degree of ionisation of $f_e > 10^{-7}$ above which an atmospheric gas can be sufficiently ionised that it may exhibit plasma behaviour. In a plasma, electron-electron interactions dominate over collisions between electrons and neutral particles, $\omega_{pe} \gg \nu_{ne}$ (Sect. 3.3.2). Additionally, for a plasma to be considered magnetized, the magnetic field must be sufficiently strong that it significantly influences the electron and ion dynamics, which we address in Sect. 5.

We now cast the results in terms of atmospheric volumes to allow a comparison between the results for different parameters. Figure 9 and 10 summarise our findings in terms of the volume fraction, $V_{\text{gas}}^{\text{th}}/V_{\text{atm}}$, with $V_{\text{gas}}^{\text{th}}$ the thermally ionised volume of the atmosphere and V_{atm} the total atmospheric volume. $V_{\text{gas}}^{\text{th}}$ is derived by calculating the fraction of the atmospheric volume for which $f_e > 10^{-7}$ (Fig. 9). Figure 10 visualises the atmospheric volume fraction where $\omega_{pe} \gg \nu_{ne}$ is fulfilled. The atmosphere volume that reached $f_e > 10^{-7}$ and satisfied $\omega_{pe} \gg \nu_{ne}$ is affected by the global parameters as follows:

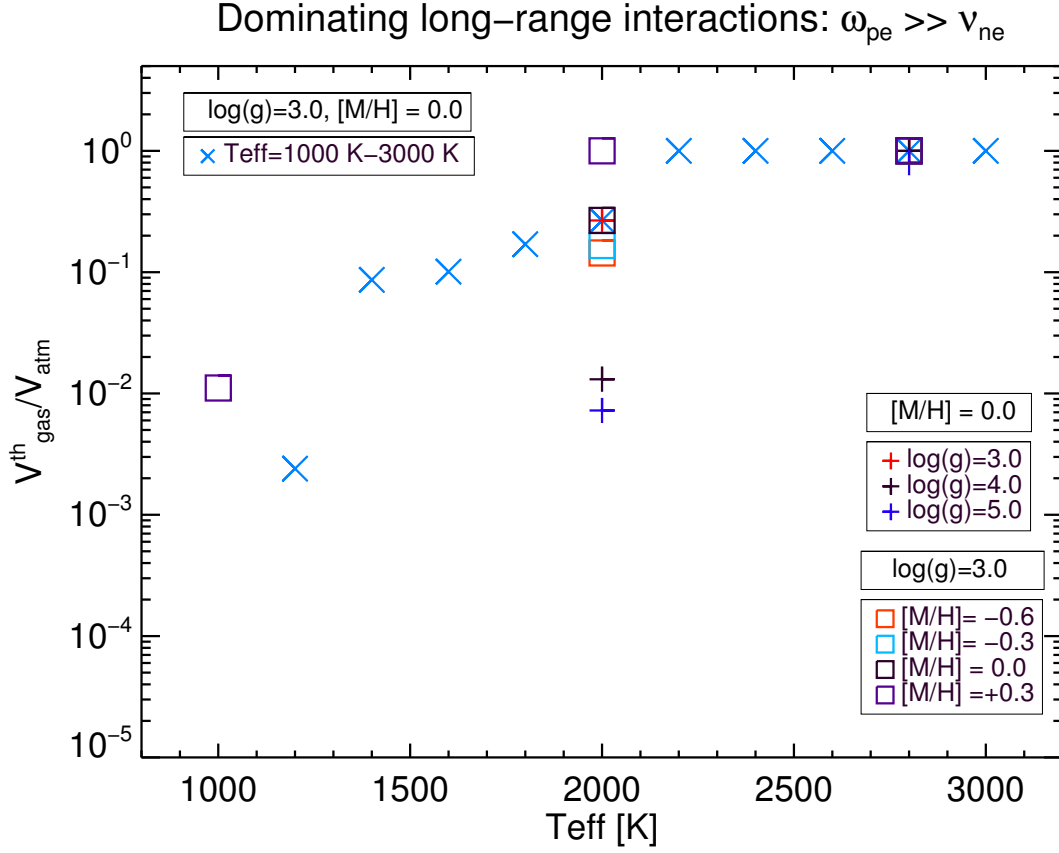


Figure 10. The fraction of the thermally ionized atmospheres volume, $V_{\text{gas}}^{\text{th}}/V_{\text{atm}}$ for $\omega_{\text{pe}} \gg \nu_{\text{ne}}$ for M-dwarf, brown dwarf and giant gas planet atmospheres.

- If T_{eff} increases, then the thermally ionised atmospheric volume fraction increases for a given $\log(g)$ and $[M/H]$.
- The $V_{\text{gas}}^{\text{th}}/V_{\text{atm}}$, that reaches $f_e > 10^{-7}$ and $\omega_{\text{pe}} \gg \nu_{\text{ne}}$, increases if $\log(g)$ decreases for a given T_{eff} and $[M/H]$.
- Higher values of the metallicity, $[M/H]$, cause a larger fraction of the atmosphere volume to have a sufficiently ionised gas that large-scale electromagnetic interactions dominate over electron-neutral collisions for a given T_{eff} and $\log(g)$.

The late M-dwarfs have the largest atmosphere volume fraction, $V_{\text{gas}}^{\text{th}}/V_{\text{atm}}$, that reached $f_e > 10^{-7}$ that is for model atmosphere structures with $T_{\text{eff}} = 2600 - 3000$ K, $\log(g)=3.0$, $[M/H] = 0.0$ and $T_{\text{eff}} = 2800$ K, $\log(g)=3.0$, $[M/H]=+0.3$. For late M-dwarfs and brown dwarfs, the atmospheric gas satisfies $f_e > 10^{-7}$ only for half of their atmosphere. For planetary objects the fraction of the volume that reaches $f_e > 10^{-7}$ becomes increasingly small except for those that have the highest value of metallicity and the lowest value of surface gravity.

Models with $2200 \text{ K} \leq T_{\text{eff}} \leq 3000 \text{ K}$, $\log(g)=3.0$, $[M/H]=0.0$ have the largest atmosphere volume fraction that reached $\omega_{\text{pe}} \gg \nu_{\text{ne}}$ for a given $\log(g)$ and $[M/H]$. Models with $T_{\text{eff}}=2800$ K, $\log(g)=4.0$, $[M/H]=0.0$; $T_{\text{eff}}=2800$ K, $\log(g)=3.0$, $[M/H]=-0.6, -0.3, 0.0, +0.3$ and $T_{\text{eff}}=2000$ K, $\log(g)=3.0$, $[M/H]=+0.3$ have the largest atmosphere volume fraction that reached $\omega_{\text{pe}} \gg \nu_{\text{ne}}$ as well. In young brown dwarfs, the atmospheric gas volume that reaches $\omega_{\text{pe}} \gg \nu_{\text{ne}}$ is more than 50%. The atmospheric gas volume that reaches

$\omega_{\text{pe}} \gg \nu_{\text{ne}}$ for planetary objects is smaller than for the rest of the objects, i.e. for $T_{\text{eff}} = 1000$ K, $\log(g)=3.0$, $[M/H]=+0.3$. Our results show that $V_{\text{gas}}^{\text{th}}/V_{\text{atm}}$ ($\omega_{\text{pe}} \gg \nu_{\text{ne}}$) is larger than $V_{\text{gas}}^{\text{th}}/V_{\text{atm}}$ ($f_e > 10^{-7}$) for $1000 \text{ K} \leq T_{\text{eff}} \leq 3000 \text{ K}$. A general observation is that despite a relatively low degree of ionisation, large-scale electromagnetic interactions can dominate a considerably larger atmospheric volume than a f_e evaluation would suggest for all ultra-cool objects in our sample.

4 MOST ABUNDANT THERMAL IONS IN LATE M-DWARF, BROWN DWARF AND GIANT GAS PLANET ATMOSPHERES

We investigate the atmospheric gas-phase composition regarding the most abundant local gas ions to demonstrate which are the dominating electron donors across the star-planet regime based on our non-irradiated DRIFT-PHOENIX model atmosphere grid. This investigation allows us to understand which gas-phase species are responsible for increasing the number of free electrons in ultra-cool atmospheres and consequently, responsible of satisfying the plasma parameters given in Eq.1-3. It also allows us to understand how the chemical composition of the gas is linked with the dominating electron donors in the gas-phase. In the case of cloud-forming atmospheres, the abundance of the element depleted by cloud formation has an effect on electron donors

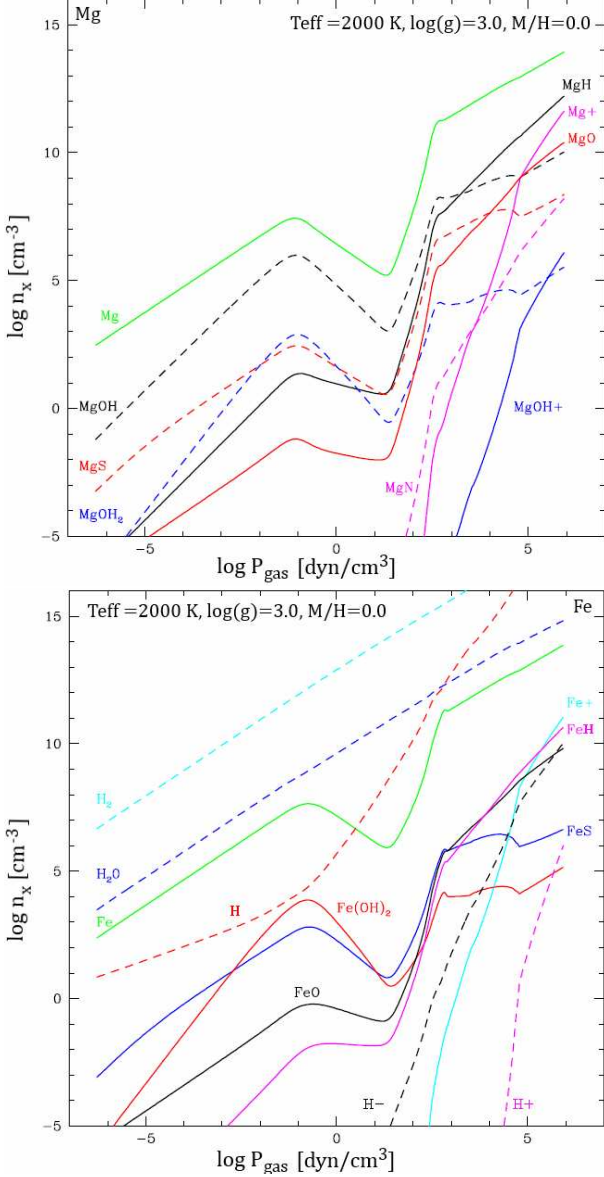


Figure 8. Same like Fig. 7. Both, Mg and Fe are influenced by dust formation which strongly decreases both elements, resulting into the localized large kink. The upper left corner contains the element considered. H-binding species are shown for comparison.

at the location of the cloud. This section serves also as reference for future investigations on ionisation processes and their effect on the gas composition like in (Rimmer & Helling 2013).

4.1 Dominating ions across the late M-dwarf, brown dwarf and planetary regime

Figure 6 demonstrates for a subset of effective temperatures $T_{\text{eff}} = 1000 \dots 3000$ K ($\log(g)=3.0$ solar element abundances) that K^+ , Na^+ , Ca^+ , Mg^+ and Fe^+ are the dominating thermal electron donors. These ionic species are the most significant contributors to the electron number density from thermal ionisation. Species that have sufficiently low first ionization potentials and sufficiently high atmospheric num-

ber densities will contribute most effectively to the thermal degree of ionization. Therefore, K^+ , Na^+ and Ca^+ provide the majority of thermal electrons. Figure 6 demonstrates that K^+ is the dominating thermal electron donor where $p_{\text{gas}} < 10^{-2}$ bar for all atmospheres except in an M-dwarf atmosphere of $T_{\text{eff}} = 3000$ K. The second dominating electron donor is Na^+ from $T_{\text{eff}} = 2000$ K. Na^+ dominates for $T_{\text{eff}} = 3000$ K. For increasing gas pressure, $p_{\text{gas}} > 10^{-2}$ bar, Na^+ and K^+ are the dominating thermal electron donor for $T_{\text{eff}} = 2000$ K, 1400 K, 1000 K. For example, Mg^+ provides most of the electrons in the $T_{\text{eff}} = 3000$ K model for $p_{\text{gas}} > 10^{-2}$ bar. The detailed results for all model groups are summarised in Tables A1 and A2 in the Appendix A.

Figures 7 and 8 show the distribution of the most important electron donating elements over atoms, molecules and ions. For example, Na^+ is the dominating Na-species at high temperature, but the atomic Na followed by NaH and NaOH contain most of the element Na at lower temperatures. Ca, Mg and Fe are involved in the formation of many molecules. In the case of Ca, CaCl_2 , CaOH and $\text{Ca}(\text{OH})_2$ reach the abundances not much lower or even higher than the atomic Ca. Our investigations show that it is not sufficient to determine the local degree of ionisation based on one prescribed electron donor species. Such an approach has been chosen in various complex simulations like MHD simulations for protoplanetary disks (e.g. Sano et al. 2000) or atmospheric circulation models (e.g. Perna, Menou & Rauscher 2010).

The exact amount with which K, Na, Ca, Mg and Fe contribute to the local degree of thermal ionisation will also depend on the amount of each element that is chemically locked in cloud particles. Element depletion by cloud formation is fully taken into account for Mg and Fe (see Sect. 2) in the DRIFT-PHOENIX atmosphere simulations. The more extended work by Helling, Woitke & Thi (2008) (Fig. 6) suggests that the effect of cloud formation on the Ca^+ abundance is negligible. Morley et al. (2012) (Fig. 3) show that $\text{Na}_2\text{S}[\text{s}]$ is thermally stable for $T_{\text{gas}} < 1100$ K and $\text{KCl}[\text{s}]$ for $T_{\text{gas}} < 900$ K, hence Na^+ and K^+ would be affected by cloud formation in a similar temperature window. The solar element abundances for Na (6.17), K (5.08) and Cl (5.5) are lower than for Ca (6.31) and it may therefore be reasonable to expect a similarly negligible effect of cloud formation on the abundances of Na^+ and K^+ .

4.2 Summary on electrostatic parameters

Our reference study suggests that:

- M-dwarfs have almost the entire atmospheric gas ionised, brown dwarfs present only an ionised gas for $p_{\text{gas}} > 10^{-4}$ bar and giant gas planets present only a small fraction of an ionised gas for values of $p_{\text{gas}} > 10^{-1}$ bar.
- Collective, long-range electromagnetic interactions of electrons dominate over short-range binary interactions with neutral particles increase as T_{eff} increases in the atmospheres of M-dwarfs and brown dwarfs. Giant gas planets are too cool to fulfill this criterion for large ranges of p_{gas} ; only for $T_{\text{eff}} = 1200$ K, $\log(g)=3.0$, $[\text{M}/\text{H}]=0.0$ and $T_{\text{eff}} = 1000$ K, $\log(g)=3.0$, $[\text{M}/\text{H}] = +0.3$ a small fraction of the atmospheric gas at most deeper parts of their atmosphere.
- $\lambda_D \ll L$ is fulfilled for M-dwarfs throughout their atmo-

spheres. For brown dwarfs only for $p_{\text{gas}} > 10^{-8}$ bar and for giant gas planets for $p_{\text{gas}} > 10^{-3}$ bar.

K^+ , Na^+ , Ca^+ , Mg^+ and Fe^+ are the dominating thermal electron donors, however, K^+ , Na^+ and Ca^+ provide the majority of electrons for $T_{\text{eff}} = 1000 \dots 3000$ K for $\log(g) = 3.0$ and solar element abundances. In particular, the degree of ionisation is low in the upper atmospheres where the abundances of those ions are low. As their abundances increase, f_e increases as well. Long-range electromagnetic interactions dominating over collisions (Eq. 2) and a zero electrostatic forces inside the plasma (Eq. 3) require a sufficient number of free charged particles. Any process (cloud formation, CR impact) that impacts the element abundance of the dominating electron donors will affect to the electric state of the atmosphere, and the potential coupling to a large-scale magnetic field.

5 MAGNETIZED PLASMA PARAMETERS ACROSS THE STAR-PLANET REGIME

In the previous sections we discussed that for a plasma to exist, the gas needs to be ionised to a certain degree ($f_e > 10^{-7}$). The plasma frequency was used to investigate where in the atmosphere, electromagnetic interactions dominate over kinetic collisions between electrons and neutrals.

The Debye length provides insight about the length scales on which electrostatic interactions influencing the atmospheric gas. We demonstrated that the atmospheric volume fraction, $V_{\text{gas}}^{\text{th}}/V_{\text{atm}}$, suspected to show plasma behaviour, varies largely through the M-dwarf to planetary regime.

A plasma is considered magnetised when the motion and dynamics of the charged particles are influenced by an ambient magnetic field. This requires that the magnetic field is of sufficient magnitude that the charged particles can on average participate in at least one Larmor orbit before colliding with a neutral atom or dust particle. Otherwise, frequent collisions with the ambient neutrals will dominate the dynamical evolution of the plasma particles and the influence of the magnetic field will be negligible. In some instances, because of the differing mass between electrons and ions, the electrons can be magnetised while the ions are not. For magneto-fluid descriptions of plasmas (such as magnetohydrodynamics) both the electrons and ions need to be magnetised. Radio flares (Route & Wolszczan 2012), X-ray flares (Berger et al. 2010) and quiescent radio emission (Williams, Berger & Zauderer 2013) have been observed in brown dwarfs, Schmidt et al. (2015) conclude that 45% of their active L-dwarfs are also variable. This fraction of L-dwarfs, which is lower compared to the 60% of active M-dwarfs that were found to be variable in their sample, lead Schmidt et al. (2015) to speculate about a brown dwarf chromosphere as origin for the observed $\text{H}\alpha$ emission and variability. These observations suggest that there should be a strong magnetic field and considerable coupling between the magnetic field and the atmospheric gas, either to directly accelerate free electrons or to allow plasma waves to travel into the low-density upper atmosphere and deposit their energy causing a chromosphere to develop. It is interesting to note here that old brown dwarfs ($\log(g) = 5.0$) have enough

time available to build up a chromosphere even if the acoustic heating rates should be low due to a insufficient magnetic coupling of the atmosphere. For young brown dwarfs, rapid rotation may favour chromospheric heating by a better coupling to a stronger magnetic field.

5.1 Cyclotron frequency versus collisional frequency $\omega_c \gg \nu_{\text{coll}}$

The cyclotron frequency is the angular velocity with which charged particles gyrate around the magnetic field line (Boyd & Sanderson 2003), $\omega_{c,s} = v_{\perp,s}/r_{L,s} = q_s B/m_s$ in $[\text{rad s}^{-1}]$, where m_s [kg], q_s [C], B [T] and $v_{\perp,s}$ [m s^{-1}] are the mass of species s , with charge q_s and speed perpendicular to the magnetic field $v_{\perp,s}$ respectively; and $|\vec{B}| = B$ is the magnitude of the external magnetic flux density present in the medium. For a charged particle's motion to be dictated by a magnetic field, the particle needs to complete on average one gyration before a collision with a neutral atom. Formally, a magnetised plasma requires

$$\omega_{c,s} \gg \nu_{\text{ns}}, \quad (7)$$

where ν_{ns} [s^{-1}] is the collision frequency for neutral particles with charged species s . From Eq. 7 we obtain the minimum value for the external magnetic field flux, $|\vec{B}| = B$, that is needed to satisfied this criteria. Applying the definitions for $\omega_{c,s}$ and ν_{ns} , we derive the critical magnetic flux density that is required for the dynamics of the charged particle to be influenced by the background magnetic field:

$$\frac{eB}{m_s} \gg \sigma_{\text{gas},e} n_{\text{gas}} v_s, \quad (8)$$

$$\Rightarrow B_s \gg \frac{m_s}{e} \sigma_{\text{gas},e} n_{\text{gas}} \left(\frac{k_B T_s}{m_s} \right)^{1/2}, \quad (9)$$

where the collision, or scattering, cross section is $\sigma_{\text{gas}} = \pi \cdot r_{\text{gas}}^2$. The atmospheric gas in late M-dwarfs, brown dwarfs and most likely also in giant gas planets is composed mostly of molecular hydrogen, H_2 . The collision cross section is approximated as $\sigma_{\text{gas}} \approx \sigma_{\text{H}_2} \approx \pi \cdot r_{\text{H}_2}^2 = 5.81 \cdot 10^{-20} \text{ m}^2$ ($r_{\text{H}_2} = 1.36 \cdot 10^{-10} \text{ m}$).

Taking the electrons and ions as the particles that are influenced by an external magnetic flux density, Eq. 9 becomes

$$B_e \gg \frac{m_e}{e} \sigma_{\text{gas}} n_{\text{gas}} \left(\frac{k_B T_e}{m_e} \right)^{1/2}, \quad (10)$$

$$B_i \gg \frac{m_i}{e} \sigma_{\text{gas}} n_{\text{gas}} \left(\frac{k_B T_i}{m_i} \right)^{1/2}. \quad (11)$$

Grouping the constants, we rewrite Eqs. 10 and 11 as $B_e \propto n_{\text{gas}} (m_e T_e)^{1/2}$, with B_e as the minimum threshold for the magnetic flux density to ensure that the electrons are magnetised and $B_i \propto n_{\text{gas}} (m_i T_i)^{1/2}$, with B_i as the minimum threshold for magnetic flux density required to ensure that an ion, i , is magnetised in Fig. 12. The ion masses, m_i , are taken to be for K^+ , Na^+ , Ca^+ , Fe^+ , and Mg^+ according to Sect. 4 assuming local thermal equilibrium, $T_{\text{gas}} \approx T_i \approx T_e$.

Figure 11 shows that for a $p_{\text{gas}} < 10^0$ bar and $B = 10^3$ G and for a $p_{\text{gas}} < 10^{-2}$ bar and $B = 10$ G, $\omega_{ce} \gg \nu_{ne}$ (horizontal black line) is reached for all model atmosphere structures. There is almost no dependence on T_{eff} , $\log(g)$ and the metallicity. Largest values of ω_{ce}/ν_{ne} are reached

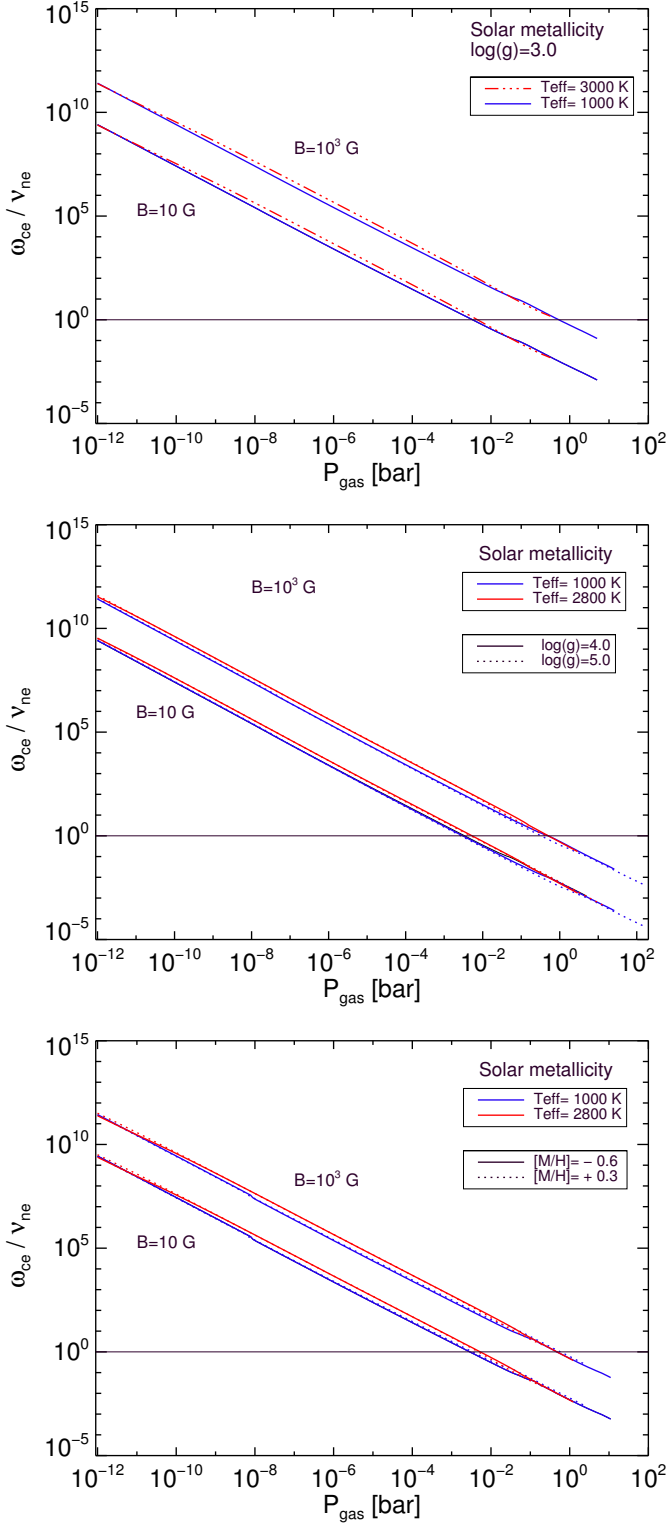


Figure 11. Ratio of cyclotron frequency of the electrons and the frequency of collisions between neutral particles and electrons. **Top:** Group 1. **Middle:** Group 2. **Bottom:** Group 3.

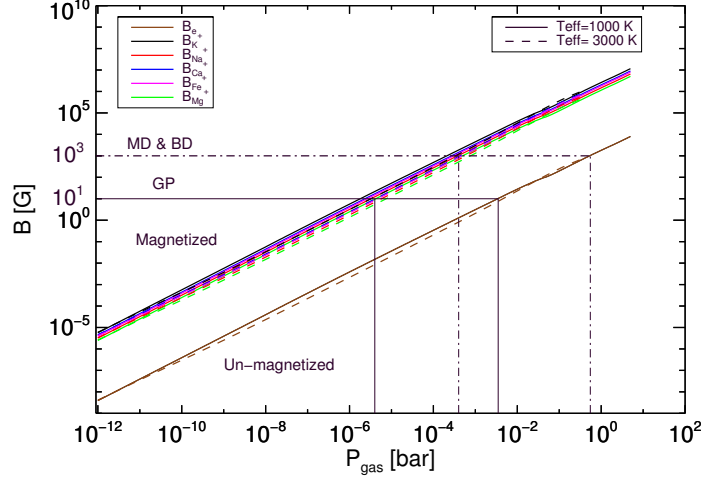


Figure 12. Magnetic flux density required for electrons, B_e (lower set of lines), and ions, B_i (upper set of lines), to be magnetically coupled to a background magnetic field in the object ($B = 10$ G – giant gas planets (GP), $B = 10^3$ G – M-dwarfs (MD), brown dwarfs (BD); black horizontal/vertical lines). If $B > B_i$ (or $B > B_e$), $\omega_{c,s} \gg \nu_{ns}$ is fulfilled and the gas is magnetised by the external magnetic field B .

for $B = 10^3$ G representative for M-dwarfs or brown dwarfs. Figure 12 shows for which atmospheric gas pressures, p_{gas} , electrons and ions can be magnetised in the atmospheres of M-dwarfs, brown dwarfs and giant gas planets. For M-dwarfs and brown dwarfs an background magnetic field flux density of $B = 10^3$ G is large enough to magnetise the charged particles: for electrons at $p_{\text{gas}} < 1$ bar and for ions at $p_{\text{gas}} < 10^{-3}$ bar. For giant gas planets, the magnetised part of the atmosphere decreases because of a smaller background field ($B \leq 10$ G) compared to M-dwarfs and brown dwarfs. For electrons this occurs at $p_{\text{gas}} < 10^{-2}$ bar and for ions at $p_{\text{gas}} < 10^{-5}$ bar. Figure 15 summarises the results on magnetic coupling in term of the affected atmospheric gas volume, $V_{\text{gas}}^{\text{th}}/V_{\text{atm}}$, that reach $\omega_{c,e} \gg \nu_{ne}$:

- If T_{eff} increases, the magnetically coupled volume of an atmosphere increases for a given $\log(g)$ and $[M/H]$.
- If $\log(g)$ decreases, then the magnetically coupled volume increases for a given T_{eff} and $[M/H]$.
- Higher values of the metallicity, $[M/H]$, cause an increase of $V_{\text{gas}}^{\text{th}}/V_{\text{atm}}$ for a given T_{eff} and $\log(g)$.

For a fixed value of magnetic flux density, M-dwarfs and brown dwarf atmospheres have the largest magnetically coupled volume. Unsurprisingly, a smaller fraction of a giant gas planets atmosphere is magnetically coupled when thermal ionisation is considered as the only source of gas ionisation. However, this fraction can reach 80% also in a planetary atmosphere. The fraction of the atmospheric gas volume, $V_{\text{gas}}^{\text{th}}/V_{\text{atm}}$, that reaches $f_e > 10^{-7}$ (Fig. 9) and $\omega_{pe} \gg \nu_{ne}$ (Fig. 10) increases for the same set of global parameters T_{eff} , $\log(g)$, $[M/H]$ like the atmospheric gas volume that reaches $\omega_{ce} \gg \nu_{ne}$. Figure 15 demonstrates also that a larger atmospheric gas volume can be expected to be magnetically coupling than the thermal degree of ionisation had initially suggested in Fig. 9. This finding is particularly relevant with

respect to the effect that the magnetic field geometry might have on the detection of the $H\alpha$ activity signatures and on the radio emission: Donati et al. (2008) show that partially-convective M dwarfs host non-axisymmetric large-scale magnetic fields with a strong toroidal component, while fully convective M dwarfs have stronger large-scale field dominated by a mainly axisymmetric poloidal component. A partial ionisation of the magnetically coupled gas does influence the magnetic flux density.

5.2 Magnetic Reynolds Number, R_m

The previous sections outlined the framework quantifying when an ionised gas in a substellar atmosphere behaves like a magnetized plasma. The magnetic Reynolds number is an easy to utilise measure of a potentially magnetically coupled ionised gas. Within the context of MHD, the magnetic Reynolds number (R_m) is the ratio of the convective and diffusive terms from the magnetic field induction equation. It quantifies whether the MHD plasma is in the ideal or resistive regimes. When the magnetic Reynolds number is very large (i.e. in the limit of large length scales), the MHD plasma is in the ideal MHD regime and the convective term has the dominant influence. In this regime the motion of the plasma fluid is determined by the magnetic field and vice versa. In the resistive MHD regime, the diffusive term is important and dissipative processes as Ohmic dissipation (Huang & Cumming 2012; Perna, Menou & Rauscher 2010) become significant. The magnetic Reynolds number is defined through the induction equation

$$\frac{\partial \vec{B}}{\partial t} = \nabla \times (\vec{u} \times \vec{B}) + \eta \nabla^2 \vec{B} \quad (12)$$

where $|\vec{B}| = B$ [T] is the magnetic flux density, u is the flow velocity (formed by electrons and ions), and σ [S m^{-1}] is the electric conductivity. The magnetic diffusivity, η , is linked to the conductivity by $\eta = 1/\sigma$ in [$\text{m}^2 \text{s}^{-1}$] and represents the diffusion of the magnetic field, a measure of the effect of collisions between the electrons and the neutral particles on the magnetic field. The collisions between the neutral particles and the charged particles (electrons or ions) have an influence on the diffusivity of the magnetic field. If the effect of the collisions is sufficient to displace them away from the magnetic lines, the coupling between the magnetic field and the fluid may be not effective. Therefore, the diffusion of the magnetic field depends on the frequency of the collisions between neutral particles and charged particles.

The magnetic Reynolds number, R_m can be defined as the ratio between the relative strength between the diffusive term and the advective term of the induction equation. It can be used as a measure of the magnetic coupling calling the plasma coupled to the magnetic field if $R_m \geq 1$, with

$$R_m = \frac{|\nabla \times (\vec{u} \times \vec{B})|}{\eta |\nabla^2 \vec{B}|}. \quad (13)$$

Applying a dimensional analyses, Eq. 13 reduces to

$$R_m \approx \frac{vB/L}{\eta B/L^2} = \frac{vL}{\eta}, \quad (14)$$

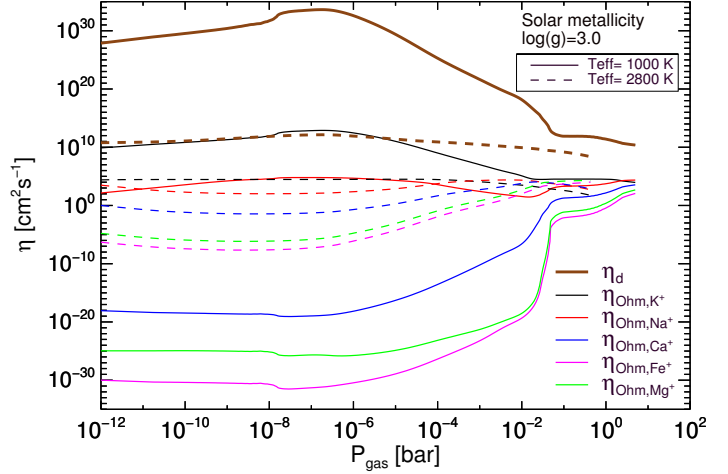


Figure 13. Decoupled diffusion coefficient, $\eta_d = c^2 \nu_{en} / \omega_{pe}^2$ and the Ohmic diffusion coefficient, $\eta_{ohm} = c^2 \nu_{ei} / \omega_{pe}^2$ for the dominating thermal electron donors for $T_{eff} = 1000, 2800$ K, for $\log(g)=3.0$ and solar element abundances; K^+ , Na^+ , Ca^+ , Fe^+ and Mg^+ (Fig. 6). The Ohmic diffusion coefficient is smaller than the decoupled diffusion coefficient. This result suggest that the binary interactions between the ions and electrons (η_{ohm}) are not significant compared to the binary interactions between electrons and neutral particles (η_d) in the case of thermal ionisation. The lines in both temperature sets appear from top to bottom in the order η_d , η_{ohm,K^+} , η_{ohm,Na^+} , η_{ohm,Ca^+} , η_{ohm,Mg^+} , η_{ohm,Fe^+} .

where L [cm] is a typical length scale of the plasma over which $|\vec{B}| = B$ varies through a hydrodynamic motion of a velocity $|\vec{v}|$, can be approximated by $L=10^3$ [m] (Helling et al. 2011). The diffusion coefficient, η , can be approximated by $\eta \approx \eta_d$ (Fig. 13).¹

Therefore, the expression for the magnetic Reynolds number is rewritten as

$$R_m \approx 10^{-4} \cdot v_{flow} \left(\frac{n_e}{n_{gas} T_e^{1/2}} \right). \quad (15)$$

The values for the flow velocity chosen are $v_{flow} = 10^4$ cm s^{-1} and $v_{flow} = 10^6$ cm s^{-1} guided by values of circulation models (Cooper & Showman 2005; Menou & Rauscher 2009; Rauscher & Menou 2013; Heng & Showman 2015; Rauscher & Kempton 2014). Figure 14 represents the magnetic Reynolds number for the DRIFT-PHOENIX model atmosphere structures which are comparable to the earlier results

¹ The diffusion coefficient used in Eq. 14 is given by $\eta = \eta_d + \eta_{ohm}$ being $\eta_d = c^2 \nu_{en} / \omega_{pe}^2$ as the decoupled diffusion coefficient and $\eta_{ohm} = c^2 \nu_{ei} / \omega_{pe}^2$ as the Ohmic diffusion coefficient and $\eta_d \gg \eta_{ohm}$. Both measure the degree of the dominance of the collisions between electrons-neutral particles and electrons-ions respectively over long-range electromagnetic collective interactions. It is easy to relate η_d with ω_{pe} / ν_{ne} (see Fig. 3). If the latter increase, the diffusion coefficient decrease and the magnetic field may be generated and transported by fluid motions allowing the magnetic energy to be released into upper layers of the atmosphere as radio, X-ray and $H\alpha$ emissions.

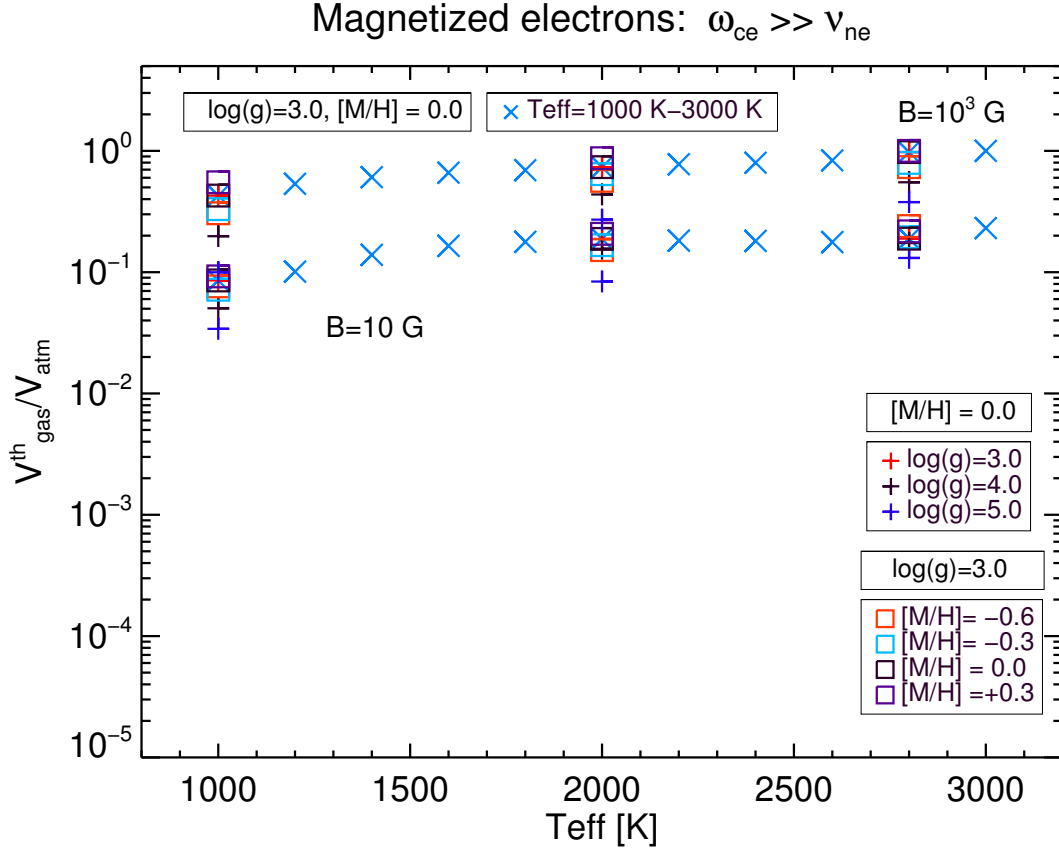


Figure 15. The fraction of the atmospheric volume, $V_{\text{gas}}^{\text{th}}/V_{\text{atm}}$, where $\omega_{\text{ce}} \gg \nu_{\text{ne}}$ for M-dwarf, brown dwarf and giant gas planet atmospheres. M-dwarfs and Brown dwarfs are represented by $B = 10^3$ G and giant gas planets for $B = 10$ G.

by Mohanty et al. (2002) that were based on DUSTY- and COND-PHOENIX:

- Reynolds number increases as T_{eff} increases because of the increasing of n_e/n_{gas} in globally and locally hotter atmospheres (see Sec. 3.3.1). The highest R_m is reached for $T_{\text{eff}} = 3000$ K, $\log(g) = 3.0$, $[M/H] = 0.0$, $v_{\text{flow}} = 10^6$ cm s $^{-1}$.
- Lower gravities cause an increased R_m for a given T_{eff} and $[M/H]$ in the inner, high-density part of the atmosphere only. However, higher gravities cause an increased R_m for a given T_{eff} and $[M/H]$ in the outer, low-density atmosphere.
- Higher values of metallicity cause a increased of R_m at high values of p_{gas} for a given T_{eff} and $\log(g)$. Low-metallicity atmospheres with low effective temperatures, i.e planet or T- and Y-dwarf atmospheres, have an increasing R_m in the outer, low density. This correlates with a drastically changing gas-phase chemistry as shown in Fig. 6.

Our results suggest that ideal MHD, where a fully ionised gas is assumed, is best suited for models atmospheres with $T_{\text{eff}} \geq 3000$ K which includes M-dwarfs and young brown dwarfs. For cooler brown dwarfs and planetary regime objects only a small fraction of their atmosphere can be considered in ideal MHD.

6 DISCUSSION

6.1 Chromospheres on ultra-cool objects

Observations in radio, soft X-ray and H_{α} wavelengths from low-mass objects infer that their atmospheres are populated with magnetized plasmas. Radio and X-ray emission from ultra-cool dwarfs have been well established by different authors (e.g. Berger (2002), Route & Wolszczan 2012, Burgasser et al. 2013). Sorahana, Suzuki & Yamamura (2014) and Schmidt et al. (2015) suggest the presence of chromospheres in brown dwarfs. Sorahana, Suzuki & Yamamura (2014) suggest that weakened H_2O ($2.7\mu\text{m}$), CH_4 ($3.3\mu\text{m}$) and CO ($4.6\mu\text{m}$) absorption in combination with moderate H_{α} emission could be linked to chromospheric activity. They represent a potential chromospheric heating by an increased, constant temperature (with $p_{\text{gas}} = nkT$) in the upper atmosphere of their UCM 1D model atmosphere which allows a considerably better data fit of their observation. Schmidt et al. (2015) use a comparable approach by replacing the outer atmospheric temperature of BT-settle model atmospheres with a chromospheric temperature structure where the start of the chromosphere, a chromospheric break and the start of the transition region are used as parameters. Metchev et al. (2015) discuss the likely correlation of magnetic spots and high-amplitude photometric variability in brown dwarfs with low surface gravity values. Williams et al.

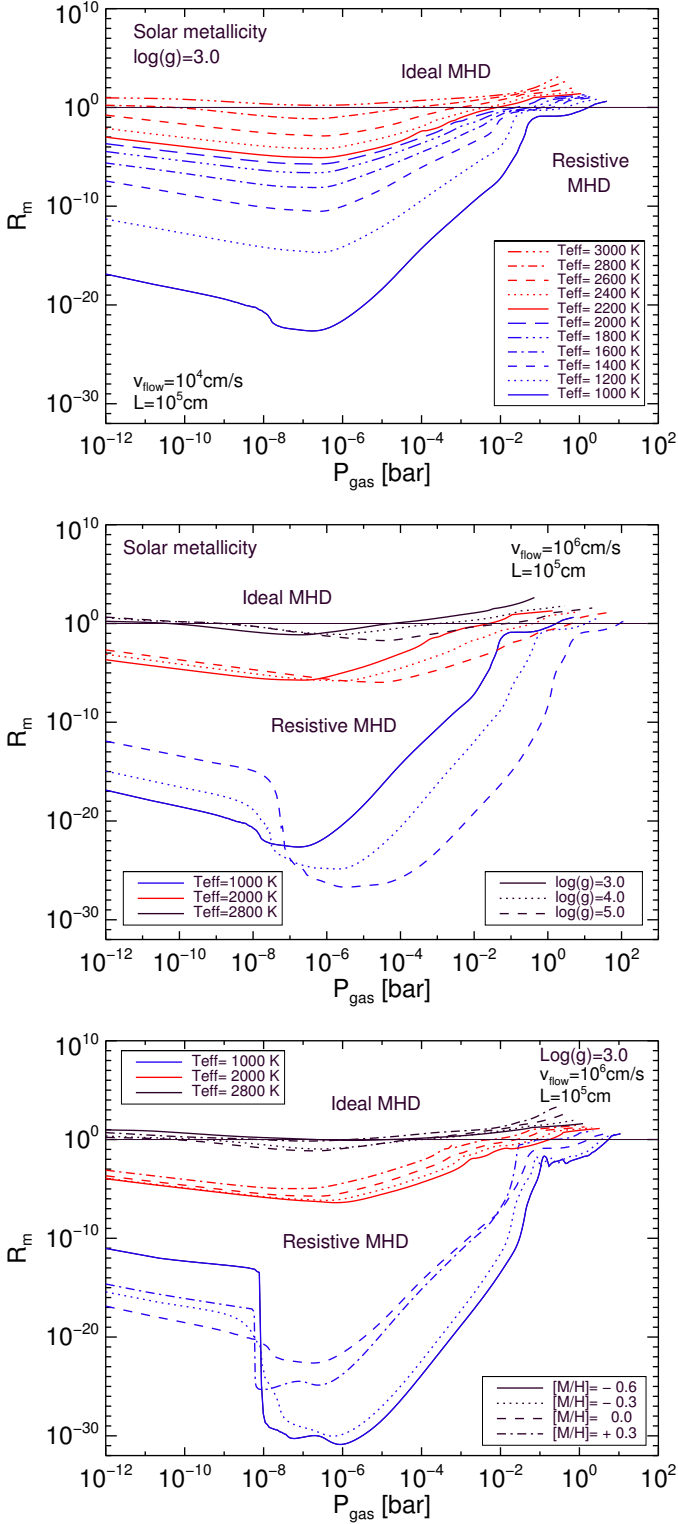


Figure 14. Magnetic Reynolds number R_m for the three different model atmosphere structure groups described in Sec 2. R_m is calculated for a flow speed of $v_{\text{flow}} = 10^6 \text{ cm s}^{-1}$. If the flow speed increases, then R_m increases. **Top:** Group 1. **Middle:** Group 2. **Bottom:** Group 3.

(2014) demonstrate that ultra-cool objects do not follow the classical Güdel-Benz relationship where the radio luminosity increases proportional to the X-ray luminosity in F – M stars (Güdel & Benz 1993). The deviation of ultra-cool stars in the Güdel-Benz relationship beyond than approximately M5 may suggest a change in the dynamo mechanism that produces the magnetic field in such ultra-cool objects (Cook, Williams & Berger 2014). Another interpretation of radio emission is the concurrence of an auroral region (Nichols et al. 2012). Speirs et al. (2014) describe a theoretical approach for cyclotron radio emission from Earth’s auroral region providing a physical description for the widely used loss cone parameterisation (e.g. Osten et al. 2015). Speirs et al. (2014) show that the radiation results from a backward-wave cyclotron-maser emission process. The radio emission is generated by electrons following a horseshoe velocity distribution, instead of a cone, that travel the magnetic field lines downward. The backwards traveling waves cause the upward refraction of the radiation which will be further enhanced by density inhomogeneities.

If the atmospheric gas is well coupled with the background magnetic field in brown dwarfs and planets, the kinetic energy carried by large-scale convective motions may be transported to the top of the atmosphere and released. Tanaka, Suzuki & Inutsuka (2014) suggest that energy from the convective part of the atmosphere might be transported through the upper atmosphere by magneto-convection processes and suggest the formation of a chromosphere by Alfvén wave heating. Mohanty et al. (2002) carried out a study of magnetic field diffusivity to explain why the chromospheric H_α activity in brown dwarfs is low in spite of being rapid rotators. Mohanty et al. (2002) based their work on a grid of model atmospheres (mid-M and L dwarfs) in a parameter range $T_{\text{eff}} = 3000 \text{ K}..1500 \text{ K}$, $\log(g)=5.0$ and $[M/H]=0.0$. They explained why in these range of T_{eff} the observation of chromospheric levels activity are lower than early M-dwarfs, considering mid-M and L dwarfs as rapid rotators. In our work, we extend our model atmosphere grid until $T_{\text{eff}} = 1000 \text{ K}$ and we include atmosphere structures with different values of $\log(g)$ and $[M/H]$ (Table 1). A linear field diffusion equation, MHD regime and LTE are used in both works. Results obtained for R_m as a measure of the ideal or resistive MHD atmosphere (see Fig. 14) could be incomplete and therefore misleading. According to Eq. 14, $R_m \propto 1/\eta$. Our results demonstrate that the regions where $R_m > 1$ satisfy also $f_e > 10^{-7}$. Atmospheres of ultra-cool objects could be ionised and treated as an ideal MHD gas only at deep layers. Furthermore, $\omega_{ce}/\nu_{ne} \gg 1$ measures the coupled between the magnetic field and the atmospheric gas and it depends, mostly, on the strength of the magnetic field (see Fig. 15). Therefore, it is possible to find large volumes of the atmospheric gas that are magnetised, but smaller magnetised volumes that are strongly ionised.

Our results further suggest not only that higher effective temperatures (in agreement with Mohanty et al. (2002)) and higher metallicity atmospheres are the best candidates for forming a magnetised atmospheric plasma in support of radio, X-ray and H_α observations in ultra-cool objects. Also low surface gravity atmospheres fall in this category which supports the interpretation by Metchev et al. (2015) that high-amplitude photometric variability in L3-L5.5 dwarfs can also be related to magnetic spot appearance.

While M-dwarfs have been shown to be fully magnetised, L-dwarfs and later brown dwarfs have smaller atmospheric volume that can be magnetised in an external magnetic field. This findings relate to the activity-vs-SpecT results in Schmidt et al. (2015) (e.g. their Fig. 6). The threshold of $T_{\text{eff}} = 2300$ K given in their Fig.6 is the Mohanty et al. (2002) threshold that points out the limit from which models $R_m > 1$ using $v = 10^4 \text{ cm s}^{-1}$ and $10^{-2} \leq \tau_J \leq 10^2$ (convection zone) being τ_J the optical length in J band. Our paper suggests that this threshold move towards $T_{\text{eff}} = 1400$ K for the same value of flow velocity and same region. This result suggests that atmospheres cooler than $T_{\text{eff}} = 2300$ K may be susceptible to be magnetized. Another criterion to consider a gas magnetised is $\omega_{ce} \gg \nu_{ne}$ (see Fig.11). For all models considered in this study (Table 1) the atmospheric gas fulfill $\omega_{ce} \gg \nu_{ne}$ for $p_{\text{gas}} < 1$ bar. Combining both criteria $\omega_{ce} \gg \nu_{ne}$ and $R_m > 1$, a large fraction of possible active objects are found for $T_{\text{eff}}=3000$ K-1400 K, $\log(g)=3.0$, $[M/H]=0.0$ (Group1).

6.2 Ionisation through non-thermal processes

Our work focuses on determining global parameters to provide the suitable local atmospheric conditions for a magnetised plasma to be present. The results suggest that ultra-cool atmospheres are susceptible to plasma and magnetic processes even if only thermal ionisation processes are considered and the influence of dust beyond element depletion is neglected. An atmospheric plasma regime and magnetised gas were found in the where M-dwarf atmosphere, which cooler brown dwarfs and planetary objects require high p_{gas} , hence, their magnetised volume is smaller than in M-dwarf atmospheres.

Additional potentially non-thermal ionisation processes will enhance the degree of ionisation and increase the local volume affected by a magnetic field. Local enhancement can result from dust-dust collisions in large cloud areas (Helling, Jardine & Mokler 2011) and Alfvén ionisation if the local, hydrodynamic wind speed is high enough (Stark et al. 2013). Electric storms that develop inside an atmosphere effects the extent of an ionosphere causing a link between the local ionisation processes and the global effects (Luque et al. 2014). Irradiation from a host star for close-in exoplanets or in white dwarfs - brown dwarf binaries (Casewell et al. 2013) will increase the local thermal ionisation globally. Galactic cosmic rays increase the number of free charge particles in single brown dwarfs. Cosmic rays are effective at ionising the upper atmospheric parts, however, the exact amount is hard to quantify without extensive chemistry simulations (Rimmer & Helling 2013).

7 CONCLUSIONS

We present a reference study for late M-dwarfs, brown dwarfs and giant gas planet to identify which ultra-cool objects are most susceptible to atmospheric gas-phase plasma processes. Only thermal ionisation is considered for this reference study and the influence of dust beyond element depletion is neglected. The effect of additional processes like cosmic ray ionisation, irradiation, Alfvén ionisation, lighting can be evaluated against the reference results in this paper.

Ultra-cool atmospheres with high T_{eff} , high $[M/H]$ and low $\log(g)$ have large fraction of atmospheric volume where plasma processes occur, and are therefore the best candidates for radio, X-ray and H_α emissions. M-dwarfs have a considerable degree of ionisation throughout the whole atmosphere, the degree of thermal ionisation for a L-dwarf is low but high enough to seed other local ionisation processes like Alfvén ionisation or lightning discharges. Electromagnetic interaction dominates over electron-neutral interactions also in regions of a very low degree of ionisation in most model atmospheres in our sample. The relevant length scales effected by electromagnetic interactions in the gas phase are larger in low-density regions of any atmosphere. The minimum threshold for the magnetic flux density required for electrons and ions to be magnetised is smaller than typical values of the global magnetic field strengths of a brown dwarf and a giant gas planet. A considerably lower magnetic flux density is required for magnetic coupling of the atmosphere in the rarefied upper atmosphere than in the dense inner atmosphere. Na^+ , K^+ and Ca^+ are the dominating electron donors in low-density atmospheres (low $\log(g)$, solar metallicity) independent of T_{eff} . Mg^+ and Fe^+ dominate the thermal ionisation in the inner parts of M-dwarf atmospheres. Molecules remain unimportant for thermal ionisation. Chemical processes (e.g. cloud formation, cosmic ray ionisation) that affect the abundances of Na, K, Mg, Ca and Fe will have a direct impact on the state of ionisation in ultra-cool atmospheres.

Our results suggest that it is not unreasonable to expect ultra-cool atmospheres (M-dwarfs and brown dwarfs) to emit H_α or even in radio wavelength as in particular the rarefied upper parts of the atmospheres fulfill plasma criteria easily despite having low degrees of ionisation. Our results therefore suggest that an ionosphere may emerge also in brown dwarf and giant gas planet atmospheres, and that the built-up of a chromosphere is likely. Both effects will contribute to atmospheric weather features and to space weather occurrences in extrasolar, planet-like objects. Ultra-cool atmospheres could also drive auroral emission without the need for a companion's wind or an outgassing moon.

ACKNOWLEDGMENTS

We highlight financial support of the European Community under the FP7 by the ERC starting grant 257431. We thank G. Lee, G. Hodósan, I. Vorgul and I. Leonhardt for valuable discussions of the manuscript. Most literature search was performed using the ADS. We acknowledge our local computer support highly.

REFERENCES

- Antonova A., Hallinan G., Doyle J. G., Yu S., Kuznetsov A., Metodieva Y., Golden A., Cruz K. L., 2013, *A&A*, 549, A131
- Benz A. O., Güdel M., 1994, *A&A*, 285, 621
- Berger E., 2002, *ApJ*, 572, 503
- Berger E. et al., 2010, *ApJ*, 709, 332
- Biller B. A. et al., 2013, *ApJL*, 778, L10
- Boyd T., Sanderson J., 2003, *The physics of plasmas* (Cambridge)

- Buenzli E., Apai D., Radigan J., Reid I. N., Fplateau D., 2014, *ApJ*, 782, 77
- Burgasser A. J., Melis C., Zauderer B. A., Berger E., 2013, *ApJL*, 762, L3
- Burgasser A. J., Putman M. E., 2005, *ApJ*, 626, 486
- Burrows A., Hubbard W. B., Lunine J. I., Liebert J., 2001, *Rev. Mod. Phys.*, 73, 719
- Casewell S. L., Burleigh M. R., Lawrie K. A., Maxted P. F. L., Dobbie P. D., Napiwotzki R., 2013, *Mem. Societa Astronomica Italiana*, 84, 1022
- Christophorou L. G., Olthoff J. K., 2004, *Fundamental electron interactions with plasma processing gases*. Springer
- Cook B. A., Williams P. K. G., Berger E., 2014, *ApJ*, 785, 10
- Cooper C. S., Showman A. P., 2005, in *Bulletin of the American Astronomical Society*, Vol. 37, AAS/Division for Planetary Sciences Meeting Abstracts #37, p. 671
- Cravens T. E., 1997, *Physics of Solar System Plasma*. Cambridge University Press
- Crossfield I. J. M. et al., 2014, *Nature*, 505, 654
- Diver D. A., 2001, *A plasma formulary for physics, technology, and astrophysics*. Wiley-VCH
- Donati J.-F. et al., 2008, *MNRAS*, 390, 545
- Duru F., Gurnett D. A., Morgan D. D., Modolo R., Nagy A. F., Najib D., 2008, *Journal of Geophysical Research (Space Physics)*, 113, 7302
- Fridman A., 2008, *Plasma chemistry*. Cambridge University Press
- Gibson N. P. et al., 2012, *MNRAS*, 422, 753
- Grevesse N., Asplund M., Sauval A. J., 2007, *Space Science Reviews*, 130, 105
- Güdel M., Benz A. O., 1993, *ApJL*, 405, L63
- Hallinan G., Antonova A., Doyle J. G., Bourke S., Briske W. F., Golden A., 2006, *ApJ*, 653, 690
- Hallinan G., Antonova A., Doyle J. G., Bourke S., Lane C., Golden A., 2008, *ApJ*, 684, 644
- Hauschildt P. H., Baron E., 1999, *Journal of Computational and Applied Mathematics*, 109, 41
- Helling C., Casewell S., 2014, *ARA&A*, 22, 80
- Helling C., Dehn M., Woitke P., Hauschildt P. H., 2008, *ApJL*, 675, L105
- Helling C., Jardine M., Mokler F., 2011, *ApJ*, 737, 38
- Helling C., Jardine M., Stark C., Diver D., 2013, *ApJ*, 767, 136
- Helling C., Jardine M., Witte S., Diver D. A., 2011, *ApJ*, 727, 4
- Helling C., Woitke P., 2006, *A&A*, 455, 325
- Helling C., Woitke P., Thi W.-F., 2008, *A&A*, 485, 547
- Heng K., Showman A. P., 2015, *Annual Review of Earth and Planetary Sciences*, 43, 509
- Huang X., Cumming A., 2012, *ApJ*, 757, 47
- Inan U. S., Golkowski M., 2010, *Principles of Plasma Physics for Engineers and Scientists*. Cambridge University Press
- Kremer J. P., Pedersen T. S., Lefrancois R. G., Marksteiner Q., 2006, *Phys. Rev. Lett.*, 97, 095003
- Luque A., Dubrovín D., Gordillo-Vázquez F. J., Ebert U., Parra-Rojas F. C., Yair Y., Price C., 2014, *Journal of Geophysical Research (Space Physics)*, 119, 8705
- Lynch C., Mutel R. L., Güdel M., 2015, *ApJ*, 802, 106
- McLean M., Berger E., Reiniers A., 2012, *ApJ*, 746, 23
- Menou K., Rauscher E., 2009, *ApJ*, 700, 887
- Metchev S. A. et al., 2015, *ApJ*, 799, 154
- Mohanty S., Basri G., Shu F., Allard F., Chabrier G., 2002, *ApJ*, 571, 469
- Morley C. V., Fortney J. J., Marley M. S., Visscher C., Saumon D., Leggett S. K., 2012, *ApJ*, 756, 172
- Nichols J. D., Burleigh M. R., Casewell S. L., Cowley S. W. H., Wynn G. A., Clarke J. T., West A. A., 2012, *ApJ*, 760, 59
- Osten R. A., Melis C., Stelzer B., Bannister K. W., Radigan J., Burgasser A. J., Wolszczan A., Luhman K. L., 2015, *ApJL*, 805, L3
- Perna R., Menou K., Rauscher E., 2010, *ApJ*, 724, 313
- Pont F., Knutson H., Gilliland R. L., Moutou C., Charbonneau D., 2008, *MNRAS*, 385, 109
- Rauscher E., Kempton E. M. R., 2014, *ApJ*, 790, 79
- Rauscher E., Menou K., 2013, *ApJ*, 764, 103
- Rimmer P. B., Helling C., 2013, *ApJ*, 774, 108
- Route M., Wolszczan A., 2012, *ApJL*, 747, L22
- Sano T., Miyama S. M., Umebayashi T., Nakano T., 2000, *ApJ*, 543, 486
- Schmidt S. J., Hawley S. L., West A. A., Bochanski J. J., Davenport J. R. A., Ge J., Schneider D. P., 2015, *AJ*, 149, 158
- Shulyak D., Seifahrt A., Reiniers A., Kochukhov O., Piskunov N., 2011, *MNRAS*, 418, 2548
- Sing D. K. et al., 2015, *MNRAS*, 446, 2428
- Sorahana S., Suzuki T. K., Yamamura I., 2014, *MNRAS*, 440, 3675
- Speirs D. C., Bingham R., Cairns R. A., Vorgul I., Kellett B. J., Phelps A. D. R., Ronald K., 2014, *Phys. Rev. Lett.*, 113, 155002
- Stark C. R., Helling C., Diver D. A., Rimmer P. B., 2013, *ApJ*, 776, 11
- Tanaka Y. A., Suzuki T. K., Inutsuka S.-i., 2014, *ApJ*, 792, 18
- Testa P., Saar S., Drake J., 2015, *Royal Society of London Philosophical Transactions Series A*, 373, 40259
- Trotignon J. G., Séran H.-C., Béghin C., Meyer-Vernet N., Manning R., Grard R., Laakso H., 2001, -, 49, 155
- Williams P. K. G., Berger E., Irwin J., Berta-Thompson Z. K., Charbonneau D., 2014, *ApJ*, 799, 192
- Williams P. K. G., Berger E., Zauderer B. A., 2013, *ApJL*, 767, L30
- Witte S., Helling C., Barman T., Heidrich N., Hauschildt P. H., 2011, *A&A*, 529, A44
- Witte S., Helling C., Hauschildt P. H., 2009, *A&A*, 506, 1367
- Woitke P., Helling C., 2003, *A&A*, 399, 297
- Woitke P., Helling C., 2004, *A&A*, 414, 335
- Yaroshenko V. V., Miloch W. J., Vladimirov S., Thomas H. M., Morfill G. E., 2011, *Journal of Geophysical Research (Space Physics)*, 116, 12218

APPENDIX A: MOST ABUNDANT THERMAL IONS IN M-DWARF, BROWN DWARF AND GIANT GAS PLANET ATMOSPHERES

Varying T_{eff} and $\log(g)$: Table A1 includes model atmospheres where $[M/H]$ is kept at a constant value of 0.0 and T_{eff} is varied alongside $\log(g)$ (see Sec. 4). The ions shown in the table are the most abundant; it does not include ions that are very prominent but not the most abundant. Note: When there are two ions listed (for example, Al^+/Na^+) the second ion occurs at the higher pressure.

Higher values of $\log(g)$ correspond to higher overall values of pressure, due to the increased surface gravity.

It is worth noting that there are other ions which are highly prominent within these models, however the following tables only show which ones are the most prominent.

Varying T_{eff} and $[M/H]$ Table A2 shows model atmospheres where $\log(g)$ has been kept at a constant value of 3.0 and T_{eff} is varied alongside $[M/H]$.

Table A1. First, second and third ion represent the most abundant positive ion in the high, middle and lower pressure regions respectively. First ion corresponds to the higher pressure (and therefore higher abundances) and visa verse.

Teff log(g)		3.0		4.0		5.0			
1000	K ⁺ Na ⁺	K ⁺	K ⁺	K ⁺ Na ⁺	K ⁺	K ⁺	K ⁺ Na ⁺	K ⁺	K ⁺
1200	K ⁺ Na ⁺	K ⁺	K ⁺						
1400	K ⁺ Na ⁺	K ⁺	K ⁺						
1600	Na ⁺	K ⁺	K ⁺						
1800	Na ⁺	K ⁺	K ⁺						
2000	Na ⁺ Ca ⁺	K ⁺	K ⁺	Na ⁺	K ⁺	K ⁺	Na ⁺	K ⁺	K ⁺
2200	Na ⁺	K ⁺	K ⁺						
2400	Na ⁺ Mg ⁺	K ⁺	K ⁺						
2600	Mg ⁺ Na ⁺	K ⁺ Na ⁺	K ⁺						
2800	Mg ⁺ Na ⁺	K ⁺ Na ⁺	K ⁺	Na ⁺ Mg ⁺	K ⁺ Na ⁺	K ⁺	Na ⁺ Mg ⁺	K ⁺	K ⁺
3000	Na ⁺ Mg ⁺ H ⁺	K ⁺ Na ⁺	Na ⁺ K ⁺						

APPENDIX B: PLASMA PARAMETER: NUMBER OF PARTICLES IN A DEBYE SPHERE: $N_D \gg 1$

A plasma has the capacity to screen a single charged particle placed at any point. That means that any single charged particle attracts oppositely charged particles producing a screening and repels those who have the same charge. A net space is produced in the neighbourhood of any single charged particle, reducing the electric field generated by it. The effective range of the net force between particles is restricted to the order of the Debye length (see Sec. 3). As a consequence, a test particle in the Debye sphere interacts only with particles that lie within this sphere. N_D measured the efficiency of this screening and allows us to calculate how many gas particles are required to participate. Hence, only particle inside this screening areas (λ_D) can be considered as electrostatically active.

All particles have a thermal velocity due to the temperature of the plasma. The deflected angle due to the electrostatic interactions is bigger if the number of particles around of the screened particle in the Debye sphere is small. The movement of the screened particle will not be smooth, unlike in the situation when the number of particles in the Debye sphere is sufficiently large to reduce it. That is why the Debye length increases as the number of particles in the screened sphere decreases. This is demonstrated in Fig. 4 where all Debye length increase with height in the atmosphere, i.e. with the outward decreasing local gas pressure.

The change in velocity due to the interactions with the particles produces a non-negligible net electrostatic force inside the Debye sphere. Therefore, large numbers of particles that are uniformly distributed inside the Debye sphere are required to avoid a large-angle deflection on a test particle. Hence the Debye length will be small in comparison to the length scale of the plasma. In this case, the plasma is dominated by many long-range interactions, rather than the short-range binary collisions of a neutral gas. A measure of the efficiency of the screening is the plasma parameter N_D .

The plasma parameter is defined as

$$N_D = (4/3)\pi n_e \lambda_D^3, \quad (\text{B1})$$

the number of particles in a Debye sphere with radius λ_D and centred on a single charge particle that produced the charge imbalance. When there are many plasma particles in a Debye sphere ($N_D \gg 1$) and long-range collective interactions are dominant over short-range collisions, the plasma frequency is much larger than the electron-ion collision frequency. Figure B1 shows $N_D \gg 1$ for all model atmosphere structures. This indicates that thermal electrons interact over large distances in atmosphere of ultra-cool atmospheres.

This paper has been typeset from a \LaTeX file prepared by the author.

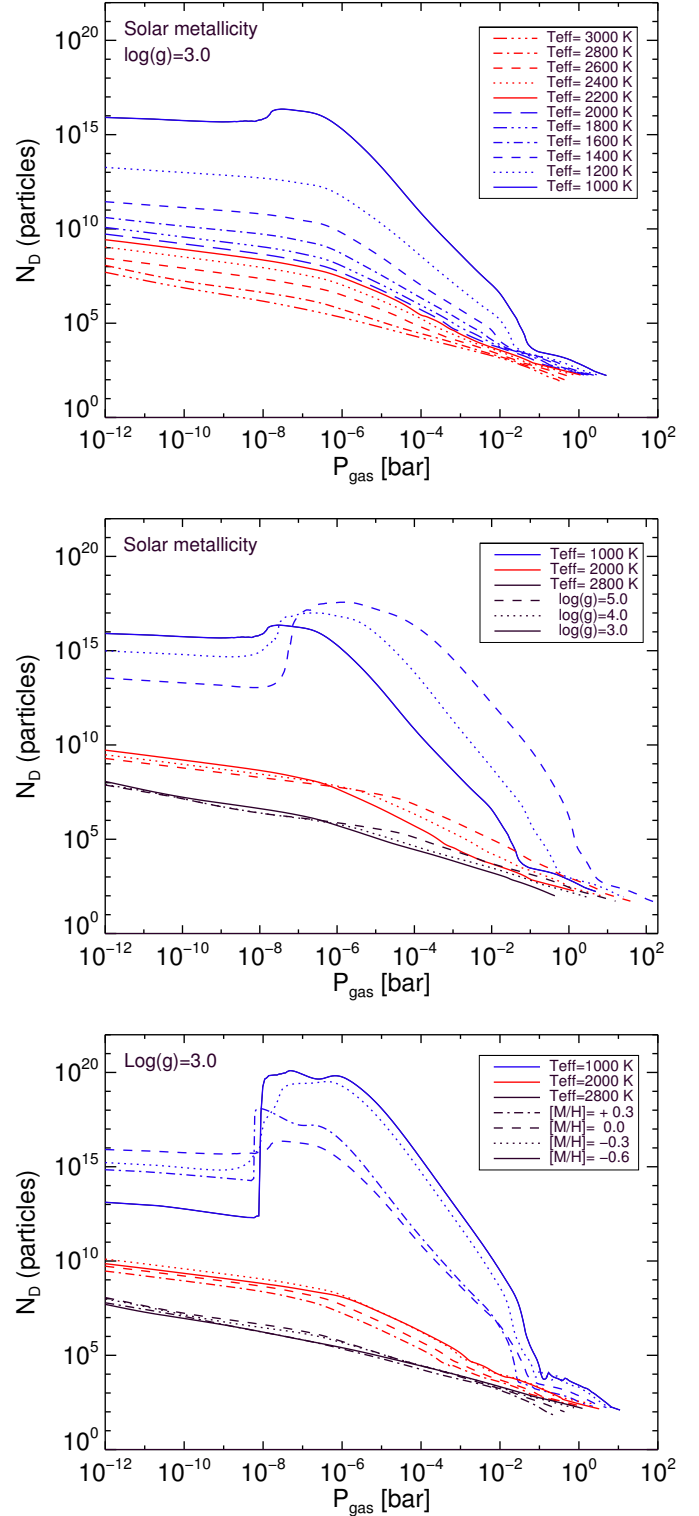


Figure B1. Number of particles inside of Debye sphere measure the efficiency of the screening given by the Debye sphere in the plasma. $N_D \gg 1$ results in the collective interactions dominate over short-range collisions in the gas. **Top:** Group 1. **Middle:** Group 2. **Bottom:** Group 3.

Table A2. First, second and third ion represent the most abundant positive ion in the high, middle and lower pressure regions respectively. First ion corresponds to the higher pressure (and therefore higher abundances) and visa verse.

M/H Teff	-0.6			-0.3			0.0			+0.3		
1000	K ⁺ Na ⁺	K ⁺	K ⁺	K ⁺ Na ⁺	K ⁺	K ⁺	K ⁺ Na ⁺	K ⁺	K ⁺	K ⁺ Na ⁺	K ⁺	K ⁺
1200							K ⁺ Na ⁺	K ⁺	K ⁺			
1400							K ⁺ Na ⁺	K ⁺	K ⁺			
1500										K ⁺ Na ⁺	K ⁺	K ⁺
1600							Na ⁺	K ⁺	K ⁺			
1800							Na ⁺	K ⁺	K ⁺			
2000	Na ⁺	K ⁺	K ⁺	Na ⁺	K ⁺	K ⁺	Na ⁺	K ⁺	K ⁺	Na ⁺	K ⁺	K ⁺
2200							Na ⁺	K ⁺	K ⁺			
2400							Na ⁺	K ⁺	K ⁺			
2600							Mg ⁺ Na ⁺	K ⁺ Na ⁺	K ⁺			
2800	Na ⁺ Ca ⁺	K ⁺ Na ⁺	Na ⁺ K ⁺	Na ⁺ Ca ⁺ K ⁺	K ⁺ Na ⁺	K ⁺	Na ⁺ Mg ⁺	K ⁺ Na ⁺	K ⁺	Na ⁺ Mg ⁺	K ⁺ Na ⁺	K ⁺
3000							Na ⁺ Mg ⁺ H ⁺	K ⁺ Na ⁺	Na ⁺ K ⁺			